A Preliminary Water Balance Model for the Tigris and Euphrates River System

Alan L. Flint[1], Lorraine E. Flint[1], Jennifer A. Curtis[2], and David C. Buesch[3]

[1]U.S. Geological Survey, Sacramento, CA

[2]U.S. Geological Survey, Eureka, CA

[3]U.S. Geological Survey, Henderson, NV

Introduction

The Tigris and Euphrates Rivers have made Iraq into the “Breadbasket of the Mideast” and allowed the development of Sumeria, the world's earliest known civilization (figure 1). Though irrigation canals were used earlier, an irrigation network including diversion dams and a 70-km aqueduct was in place by 690 B.C. (Krasny and others, 2006). Archaeologists believe that the high point in the development of the irrigation system occurred about 500 A.D., when a network of irrigation canals permitted widespread cultivation that made the river basin into a regional granary (Metz, 1988). Successive invasions and neglect led to the deterioration and partial abandonment of the irrigation and drainage system. Not until the twentieth century did Iraq make a concerted effort to restore the irrigation and drainage network and to control seasonal flooding (Metz, 1988). In 2006, about 25 percent of Iraq was irrigated by surface water (Krasny and others, 2006).

About half of Iraq’s total cultivated area is in the northeastern plains and mountain valleys, where sufficient rain falls to sustain agriculture via surface and groundwater use. The remainder of the cultivated land is in the valleys of the Euphrates and Tigris Rivers, which in Iraq receive scant rainfall and rely instead on irrigation water diverted from the rivers. Both rivers are fed by snowpack and rainfall in eastern Turkey and in northwest Iran. The rivers' discharge peaks in March and in May, too late for winter crops and too early for summer crops. The flow of the rivers varies considerably every year. Destructive flooding, particularly of the Tigris, is not uncommon, and conversely, years of low flow make irrigation and agriculture difficult.

The majority of the water that flows through the Tigris and Euphrates River basins originates outside the borders of Iraq. Therefore, the calculation of the water balance of these river systems necessitates an

understanding of the climate and environmental conditions of the entire system that extends from Turkey in the headwaters of both rivers, to Syria and Saudi Arabia in the south west, and to Iran where the Karun flows into the Shatt al Arab near the mouth at the Persian Gulf (figure 2). Although much of the waterways flowing in Turkey and Syria are dammed, an understanding of the natural, unimpaired water balance for the extent of the Tigris Euphrates River systems (TERS) serves to provide an understanding of the long term impacts of climate. This information also provides recognition of recent changes throughout the system that may highlight locations that are more or less sensitive to changes in climate, and help to lay a foundation for long term plans for water-resource management.

Climate

Average annual precipitation in the TERS ranges from 50 to over 1,000 mm/year (figure 3), with roughly 90 percent of the annual rainfall occurring between November and April, and most of it in the winter months from December through March. However, potential evapotranspiration ranges from about 800 to over 1,400 mm/year (figure 4) and the remaining six months, particularly the hottest ones of June, July, and August, are very dry. Mean annual minimum air temperatures range from below freezing in the north and northeast and > 15° C in the southern desert (figure 5). Mean minimum air temperatures in the winter range from near freezing in the northern and northeastern foothills and the western desert to 2-3° C and 4-5° C in the alluvial plains of southern Iraq. They rise to a mean annual maximum of 3-10° C in the mountainous north and northeast to over 30° C in the southern deserts (figure 5). In the summer mean minimum temperatures range from about 22° C to about 29° C and rise to maximums of over 40° C. Temperatures sometimes fall below freezing and have fallen as low as -14.4° C in the western desert. They are more likely, however, to go over 46° C in the summer months, and several stations have records of over 48° C (Hijmans and others, 2005).

Low precipitation and extreme heat makes much of Iraq a desert. Because of very high rates of evapotranspiration, soil and plants rapidly lose the little moisture obtained from the rain, and agricultural crops could not survive without extensive irrigation. In contrast, higher precipitation in the Zagros Mountains in northeastern Iraq provides permanent vegetation, such as oak trees, and date palms are found in the southern regions.

Snowfall plays a large part in maintaining flows that can extend into the dry season and provide irrigation and drinking water in the summer. Snowmelt helps to create conditions conducive to recharge into the subsurface where less water is lost to evapotranspiration. The majority of snow that feeds runoff and recharge in the TERS occurs in the mountains of Turkey and Iran, although there is a portion that

provides some runoff to the headwaters of the Tigris in northern Iraq (figure 6). The presence of snow and the resulting timing and patterns of snowmelt is controlled by air temperature, and thus is very sensitive to changes in air temperature. As a result snow accumulation and melt processes tend to amplify the effects of changing climate that are dominated by increases in air temperature and often accompanied by decreases in precipitation. These effects are manifested by less snow accumulation and earlier springtime snowmelt.

Study Area

The study area is 1,035,000 km^2 and covers portions of Turkey, Iran, Iraq, Syria, and Saudi Arabia (with a minor section in Jordan) (figures 1 and 2). The desert zone, an area lying west and southwest of the Euphrates River, is a part of the Arabian Desert, which covers sections of Syria, Jordan, and Saudi Arabia. The region consists of a wide, stony plain interspersed with rare sandy stretches. A widely ramified pattern of wadis--watercourses that are dry most of the year--runs from the Syrian border to the Euphrates. Some wadis are over 400 kilometers long and carry brief but torrential floods during the winter rains.

The uplands region, between the Tigris north of Samarra and the Euphrates north of Hit, is known as Al Jazirah (the island) and is part of a larger area that extends westward into Syria between the two rivers and into Turkey. Water in the area flows in deeply cut valleys, and irrigation is much more difficult than it is in the lower plain. Much of this zone is classified as desert.

The northeastern highlands begin just south of a line drawn from Mosul to Kirkuk and extend to the borders with Turkey and Iran. High ground, separated by broad, undulating steppes, gives way to mountains ranging from 1,000 to nearly 4,000 meters near the Iranian and Turkish borders. The alluvial plain begins north of Baghdad and extends to the Persian Gulf. Here the Tigris and Euphrates Rivers lie above the level of the plain in many places, and the whole area is a delta interlaced by the channels of the two rivers and by irrigation canals. Intermittent lakes, fed by the rivers in flood, also characterize southeastern Iraq. A fairly large area (15,000 square kilometers) just above the confluence of the two rivers at Qurnah and extending east of the Tigris beyond the Iranian border is marshland, the result of centuries of flooding and inadequate drainage. Although much of the marshland has been drained or has diminished as a result of drought, there are still large areas of permanent marsh, with additional areas becoming marshland only in years of great flooding.

The Euphrates originates in Turkey, is augmented by the Nahr River in Syria, and enters Iraq in the northwest. Here it is fed only by the wadis of the western desert during the winter rains. It then winds through a gorge, which varies from two to sixteen kilometers in width, until it flows out on the plain at Ramadi, where it flows to join the Tigris at Qurnah.

The Tigris also originates in Turkey but is significantly augmented by several rivers in Iraq, all of which join the Tigris above Baghdad, and the Diyala, which joins it below the city. Both the Tigris and the Euphrates break into a number of channels in the marshland area, and the flow of the rivers is substantially reduced by the time they come together at Qurnah. Moreover, the marshes act as silt traps, and the Shatt al Arab is relatively silt free as it flows south. Below Basra, however, the Karun River enters the Shatt al Arab from Iran, carrying large quantities of silt.

Methods

Application of the Basin Characterization Model

Watershed hydrology in the TERS drainages is the result of interactions between precipitation, evapotranspiration, surface water runoff, channel infiltration, and areally distributed infiltration, including direct recharge or groundwater interaction with rivers and lakes. Runoff, recharge, and changes in soil moisture conditions can be estimated using a simple monthly water balance approach. The Basin Characterization Model (BCM) is a physically-based model that calculates water balance fractions based on data inputs for topography, soil properties and depth, underlying bedrock geology, and spatially-distributed values (measured or estimated) of air temperature and precipitation (Flint and Flint 2007a, b).

The BCM calculates recharge and runoff monthly (figure 7) using a mathematical deterministic water-balance approach based on the distribution of precipitation and the estimation of potential evapotranspiration (Flint and Flint 2007a, b). The BCM relies on a rigorous hourly energy balance calculation using topographic shading and applies available spatial maps of elevation, bedrock permeability estimated from geology, soil water storage from soil databases, and precipitation and air temperature maps. The BCM can be used to identify locations and climatic conditions that generate excess water, quantifying the amount of water available either as runoff or as in-place recharge on a monthly basis.

The BCM has been calibrated regionally in the southwest United States, with climate very similar to the Middle East. Regional calibration compares simulated solar radiation and potential evapotranspiration to measured values, and simulated snow cover to MODIS snow cover data (Flint and Flint 2007b). Locally the model is calibrated to measured unimpaired streamflow data. The determination of whether excess water becomes recharge or runoff is governed in part by the underlying bedrock permeability. In locations with limited soil water storage, the higher the bedrock permeability, the higher the recharge and the lower the runoff generated for a given grid cell. In small gaged basins that generate unimpaired flows, the bedrock permeability can be adjusted to calculate a total basin discharge that matches the measured basin discharge. In the TERS, four stream gages with unimpaired flows were available (figure 2; table 1) and were used for model calibration. Properties adjusted during calibration were correspondingly distributed throughout the study area of the TERS and spatially distributed estimates of recharge and runoff were calculated for 50 years of available climate records, 1949-1999.

Temperature and precipitation are two primary drivers of physical processes acting at the watershed scale. BCM hydrologic variables sensitive to temperature include potential evapotranspiration (PET) and actual evapotranspiration (AET). BCM variables sensitive to quantities of precipitation include runoff and recharge.

Model Domain

The study area defines the limits of the model domain (figure 2) and is bounded by the topographic surface hydrology of the Tigris and Euphrates River system. As a result, all input parameters must be developed for this domain. Map inputs are all developed to correspond to the 180-m spatial resolution of the digital elevation model.

Development of Input Parameters Used in the Water Balance Model

Climate

Recharge and runoff are non-linearly related to precipitation and snow accumulation and melt (Flint, and others, 2004; Flint and Flint, 2007b). Therefore transient climate data are required for developing an understanding of that relation and developing an estimate of long term recharge and runoff for the region. Global climate data is available from several sources on the web in gridded format in various spatial and temporal resolutions. The following data was used for this study.

Precipitation, minimum and maximum air temperature

Steady-state data from WorldClim (http://worldclim.org/; Hijmans and others, 2005) is a global climate set of monthly grids and is readily available via the web. The data layers are generated through interpolation of average monthly climate data from weather stations on a 30 arc-second resolution grid (1-km), on the basis of major climate databases. Average monthly data is available for precipitation, and minimum and maximum air temperature. Although these data are steady-state they are at a fine-scale spatial resolution and were found to be useful for correcting the coarse scale data described below.

Transient precipitation and air temperature data was available through the Climatic Research Unit (CRU) and the Tyndall Centre for Climate Change Research (http://www.cru.uea.ac.uk/cru/data/hrg/) of the University of East Anglia, Norwich, U.K. The data used were CRU TS 2.1, with a spatial resolution of 0.5 degrees (51.6 km, Mitchell and Jones, 2005). Transient monthly data is available for precipitation, and minimum and maximum air temperature from 1901 to 2000.

These climate data sets are too coarse a resolution to be used directly in the BCM and therefore required downscaling to the 180-m spatial resolution for the model domain. Downscaling refers to the calculation of fine-scale information on the basis of coarser-scale information using various methods of statistical and spatial interpolation. Spatial downscaling was performed on the coarse resolution grids (1-km and 51.6-km) to produce fine resolution grids (180-m) using a model developed by Nalder and Wein (1998) modified with a “nugget effect” specified as the length of the coarse resolution grid (Flint and Flint, in review).

This technique combines a spatial Gradient and Inverse Distance Squared (GIDS) weighting to monthly point data using multiple regressions that are calculated for every grid cell for every month. Using the coarse-scale resolution digital elevation model (1-km or 51.6-km), parameter weighting is based on the location and elevation of the new fine resolution grid relative to existing coarse resolution grid cells (in this example we start with the WorldClim data) using the following equation:

$$Z = \left[\sum_{i=1}^{N} \frac{Z_i + (X - X_i) \times C_x + (Y - Y_i) \times C_y + (E - E_i) \times C_e}{d_i^2} \right] / \left[\sum_{i=1}^{N} \frac{1}{d_i^2} \right] \quad (1)$$

where Z is the estimated climatic variable at a specific location defined by easting (X) and northing (Y) coordinates, and elevation (E) respectively; Z_i is the climate variable from the 1-km grid cell i; X_i, Y_i, E_i are easting and northing coordinates and elevation of 1-km grid cell i; N is number of 1-km grid cells in a specified search radius; C_x, C_y, C_e are regression coefficients for easting, northing, and elevation; D_i is distance from the 180-m site to 1-km grid cell i and is specified to be equal to or greater than 1-km (the nugget) so that the regional trend of the climatic variable with northing, easting, and elevation within the search radius does not cause the estimate to interpolate between the closest 1-km grid cells, which causes a bull's-eye effect around any 180-m fine resolution grid cell that is closely associated or co-located in space with an original 1-km grid cell. This 180-m gridded data for average monthly precipitation and air temperature are the baseline data used to correct the transient coarse scale data from the CRU data base. The CRU data was downscaled in stages to reduce the bull's-eye effect of GIDS downscaling. The 51.6-km data was downscaled to 20-km, then those grids were downscaled to 5-km, then 1-km then 180-m. Resultant grids were smoothly blended into the 180-m grid and still maintained the spatial and elevational trends of the original coarse-scale data. These transient data were averaged in monthly values to develop a simple ratio between the CRU data and the originally finer scale WorldClim data. Once the ratio was developed for each month, it was multiplied across the transient monthly grids to "correct" those grids so that the long term average would exactly match the more data intensive high resolution WorldClim data that had been downscaled to 180-m .

To illustrate fine-scale patterns in historical changes in climate, we analyzed average annual values and the magnitude and direction of observed changes in climate and hydrology over the last century using the downscaled climate maps by applying a regression through annual averages for every grid cell to calculate the slope (rate of change) over the 50-yr time period.

Potential Evapotranspiration

Grids of potential evapotranspiration (PET) were available via the PET Early Warning and Environmental Monitoring Program of the USGS (http://earlywarning.usgs.gov/fews/middleeast/index.php) that endeavors to operate at national, regional, and international scales to support investigations in the areas of climate change, natural resource management, environmental change detection, food security monitoring, water resource assessments, and hazard identification/mitigation. The Middle East Data Portal provides data via the Famine Early Warning Systems Network for the Iraq/Tigris-Euphrates region.

The daily global PET is calculated from climate parameter data that is extracted from Global Data Assimilation System (GDAS-PET) analysis fields. The GDAS data are generated every 6 hours by the National Oceanic and Atmospheric Administration (NOAA). The GDAS fields used as input to the PET calculation include air temperature, atmospheric pressure, wind speed, relative humidity, and solar radiation (long wave, short wave, outgoing and incoming). PET is computed for each 6-hour period and then summed to obtain daily totals. A day is defined as beginning at 00 hours GMT.

The daily PET is calculated on a spatial basis using the Penman-Monteith equation (the formulation of Shuttleworth (1992) for reference crop evaporation is used). These equations were standardized in accordance with the FAO publication 56 for the 6-hourly calculations (Allen and others, 1998). The PET data have a 1 degree ground resolution (63-km) and are global in spatial extent. The transient monthly GDAS-PET data grids were available from 1948-2006. A USGS fine scale PET (Fine-PET) model (Flint and Flint, 2007a) was used to model clear sky steady-state monthly PET using the 180-m WorldClim temperature data and the 180-m DEM for the study area. This provides the fine scale influence of slope, aspect, and influence of the surrounding mountainous terrain on blocking direct beam solar radiation and diffuse radiation. The resulting average monthly Fine-PET grids were upscaled to match the average monthly GDAS-PET grids (63-km). The ratio of average monthly Fine-PET to the transient monthly GDAS-PET was calculated at the 63-km grid scale. Those grids were then downscaled in steps (similar to the precipitation) to 180-m grid resolution. The fine scale ratio of Fine-PET to GDS-PET was then multiplied by the average monthly Fine-PET grids. This approach honors the transient nature of the GDAS-PET data, which accounts for the transient climate (temperature, solar radiation, and cloudiness) but also redistributes that data over the landscape to correctly account for slope, aspect, and blocking ridges.

Geology

The purpose of compiling geologic information for application to the BCM is to estimate the saturated hydraulic conductivity (Ksat) of the surficial bedrock underlying soils. This attribute is scaled during the calibration process to partition the relative volume of water that either becomes runoff or recharge to match streamflow data in unimpaired basins, and the resulting Ksat values are used throughout the model domain. Whereas detailed geologic information was available for Iraq, the corresponding detail for the surrounding countries of Turkey, Iran, and Syria were scant, and general extrapolation on the basis of geologic age and proximity to known geology were used.

Bedrock Geology

A total of 144 formations for the country of Iraq that range in age from Paleozoic to Pliocene and lithologic features in Quaternary deposits were compiled from various reports or maps (Wayne Belcher, USGS, written commun., 2010). Only 87 formations or features are displayed on the 1:1,000,000 scale geologic map compiled by the Geological Survey of Iraq (GEOSURV, 2000) and documented in an accompanying ArcGIS file, however, some of the map units consist of groups of two or more formations. There is a wide range in types of hydrogeologic data described for formations and lithologic features that includes porosity, permeability, hydraulic conductivity, transmissivity, storage coefficient, yield, specific capacity, spring discharge, borehole discharge, groundwater recharge, and the estimated percentage of rainfall that becomes recharge (Jassim and Al-Gailani, 2006; Krasny and others, 2006). The amounts of each type of data are quite varied. Properties such as porosity, permeability, hydraulic conductivity, and transmissivity are preferred for inferring Ksat; however, the other properties were examined to establish equivalency or relative relations between units with different types of data. Of the map units that are also described in Jassim and Goff (2006), 24 map units have quantitative values for hydrogeologic properties, 17 map units have only qualitative values (such as “low” or “high”, etc.), and 13 map units have both quantitative and qualitative values.

Saturated Hydraulic Conductivity of Bedrock

In this text Ksat refers to the estimate of saturated hydraulic conductivity of the surficial bedrock underlying soils, and is generally lower than deep bedrock due to infilling of materials in fractures, carbonate deposits and other surficial deposits. This parameter can be approximated on the basis of several approaches. Measured hydraulic conductivity values, the most relevant to Ksat, were the least abundant of quantitative values. Most measured hydraulic conductivity values are assumed to be for lateral flow in the subsurface; however, there are a few values from some of the Quaternary lithologic features that have both vertical and lateral hydraulic conductivity values. For these detailed studies, horizontal values are typically 5 to 9 times as large as the vertical values; therefore, most of the values cited in Krasny and others (2006) might be an order of magnitude greater than what is appropriate for near-surface Ksat estimates. Initial estimates of Ksat were made on the basis of this information. Quantitative hydraulic conductivity values are considered the primary data; however, four other types of hydraulic conductivity values are used in this compilation; (1) hydraulic conductivity calculated from intrinsic permeability, (2) hydraulic conductivity calculated from transmissivity, (3) estimated hydraulic conductivity used for qualitative values, and (4) estimated hydraulic conductivity based on lithostratigraphic similarities.

The calculation of hydraulic conductivity from permeability was based on the relation presented in Freeze and Cherry (1979, p. 27). The calculation of hydraulic conductivity from transmissivity was based on a relation for a confined aquifer that includes the thickness of the unit (Freeze and Cherry, 1979, p. 59). The thickness values used in the calculations are from specific chapters in the Geology of Iraq (Jassim and Goff, 2006). Usually, the thickness of the "type section" was used; alternatively, a typical thickness (if described) was used.

Estimated hydraulic conductivity values used for qualitative values (such as very low, low, medium, high, and wide range) were based on generalizations of statistical summaries of various lithostratigraphic characteristics in similar formations and lithologic features. Hydraulic conductivity values for many formations and lithologic features were estimated based on lithostratigraphic similarities. The only measured hydraulic conductivity values were from the Quaternary deposits; however most lithologic types have at least some hydraulic conductivity values based on calculations from intrinsic permeability or transmissivity.

A series of digital bedrock geology maps (Pollastro and others, 1999a; Pollastro and others, 1999b; and Pawlewicz and others, 2003) were merged with the GEOSURV map of Iraq to develop the geologic map of the TERS study area. Because no specific information on lithologic properties was available for areas outside of Iraq, Ksat was extrapolated throughout Turkey (Pawlewicz and others, 2003) and the Arabian Peninsula and Iran (Pollastro, 1999a; Pollastro and others, 1999b) on the basis of generalized geologic descriptions and specific lithologic types. In general, measured, calculated, and estimated hydraulic conductivities are consistent with the ranges of values reported in Bear (1972) and Freeze and Cherry (1979).

Estimates of hydraulic conductivity are provided in Table 2. These values are likely much higher than the Ksat, however, the hydraulic conductivity estimates provide the relative magnitudes among the units, that when adjusted during calibration, maintains a semblance of the relative magnitudes for a reasonable spatial distribution. The lack of unimpaired streamflow data in basins representing all of the geologic types introduces uncertainty into the model results that is reduced by the rigor with which the original hydraulic conductivity numbers were established. The calibrated values of Ksat are shown for the lithologic units in table 2. They are spatially distributed according to the lithologic descriptions and illustrated in figure 8.

Soils

A compilation of regional and national soils data presented in the Harmonized World Soil Database V1.1 (FAO/IIASA/ISRIC/ISSCAS/JRC, 2009) was used to derive soil physical properties for the TERS model domain. The Harmonized World Soil Database (HWSD) consists of a 30 arc-second (~1 km) raster image and an attribute database in Microsoft Access 2003 format and provides standardized soil parameters for both topsoil (0 to 30 cm) and subsoil units (30 to 100 cm). Within the HWSD the GIS raster image file is linked to the attribute database using the harmonized soil mapping unit. Each soil mapping unit consists of one or more soils identified by a unique database identifier and the percentage of each mapping unit occupied by a given soil is provided.

Development of Soil Hydraulic Properties and Depth

The HWSD raster image was clipped to the study area boundary, a list of study area soil mapping units created, and a database query performed to extract textural and bulk density data for each soil mapping unit. The query generated a table of data for each soil mapping unit that included the soil identifier, percent of mapping unit occupied by each soil, soil depth, and textural and bulk density data for both the topsoil and subsoil. Weighted average calculations addressed spatial variations of soil properties within each mapping unit and enabled derivation of representative textural and bulk density values for the entire soil mapping unit profile. The weighted average textural estimates for each mapping unit were then used to estimate soil hydraulic properties using Rosetta V1.0 (Schaap and others, 2001), a software program that utilizes a pedotransfer function method and surrogate soil textural (percent sand, silt and clay) and bulk density data to estimate water retention parameters according to van Genuchten (1980). Outputs from Rosetta (residual water content, saturated water content, and van Genuchten curve fit parameters, α, and n) were used to estimate weighted average field capacity (water content at 0.03 MPa) and permanent wilting point (water content at 1.5 MPa) for each mapping unit. Weighted average bulk density estimates were used to estimate porosity for each soil mapping unit assuming a particle density of 2.65 Mg/m^3.

Soil depth was also required to calculate the water balance within the study area, however, soil descriptions within the HWSD database were limited to 1-meter deep profiles. Deep soils and unconsolidated alluvial units exist throughout the study area, thus accurate depiction of soil water storage required additional analysis of soil and alluvial thicknesses. Using the geologic map of the study area

described above, Quaternary alluvial units were identified and the database queried to create a map of alluvial units which was then used to identify soil mapping units underlain by Quaternary sediments.

The study area was separated into four geomorphic providences: Desert Steppe, Mesopotamian Plain, Foothills, and Mountainous Regions (figure 8) based on average annual precipitation (figure 3) and topographic relief (figure 1) (Lees and Falcon, 1952; Buringh, 1960; Adnan and others, 2006; Krasny and others, 2006). There is a strong precipitation gradient across the study area with average annual precipitation of less than 50 mm/yr in the southern deserts to more than 1,000 mm/yr in the northern mountains. The Desert Steppe and Mesopotamian Plain receive significantly less precipitation than the Foothills and Mountainous Regions. The Desert Steppe is characterized by minimal vegetation thereby enabling wind and water to erode and deflate alluvial surfaces resulting in shallow soils; however thick aeolian units (35-m high dunes) are common in the Arabian Desert located in the southwestern portion of the study area. The Mesopotamian Plain and Desert Steppe providences are separated by the Euphrates Boundary Fault and alluvial thicknesses within the Mesopotamian Plain are further influenced by tectonic subsidence. Within the Mesopotamian Plain alluvial thicknesses progressively increase eastward of the boundary fault until the Foothills Region is reached where thick alluvial fans form at the base of the Mountainous Region. The transition from foothills to mountains is characterized by a significant increase in topographic relief. Soils in this region are typically shallow and deep alluvial units are limited to mountain valleys.

The next step in developing the soil depth for each mapping unit was based on geomorphic providence, an isopach map of alluvial thickness (Figure 15.2; Adnan and others, 2006), parent material, and soil profile depths from the HWSD database. If the mapping unit was within the Mesopotamian Plain or the Arabian Desert and the assigned parent material from the bedrock geology map was Quaternary alluvium, a soil depth of 6 meters was assigned. Previous studies of infiltration in desert environments (Flint and Flint, 2007a) indicate 6 meters is a reasonable assumption for the maximum penetration depth of the wetting front and thus represents a limiting infiltration condition. All other mapping unit soil depths were estimated using a weighted average calculation. The table of properties for each mapping unit, generated during the original HWSD database query, shows that many of the mapping units were composed of a percentage of shallow soils. A weighted average calculation was performed for mapping units with shallow soils. For example, if the soil depth for 40 percent of a mapping unit was 0.1 meters and the soil depth for the remaining 60 percent was 1 meter, the estimated soil depth for the mapping unit was 0.68 m.

The final step in producing more discrete spatial resolution for this relatively coarse representation of soil depth was to use the general relation of soil depth to slope that is reflected in mountainous regions and described above in general terms. In the mountainous regions of the model domain it was assumed that the soil was shallower when the slopes were greater. To develop a revised soil thickness map using the 180-m elevation grid, a calculation was made that assumed that if the percent slope was greater than 35 percent the estimated soil thickness was multiplied by 0.4. If the slope was less than 35 percent but greater than 15 percent, the soil thickness was multiplied by 0.6. This final soil depth map is shown in figure 9 and illustrates the finer resolution in depth in the mountainous regions, deeper soils in the alluvial plain, especially in the areas around the Tigris and Euphrates Rivers.

After estimating field capacity, permanent wilting point, porosity and soil depth for each mapping unit these parameters were incorporated into the attribute table of the HWSD raster image. From this attributed raster image a series of grid files with a 180-m cell size were generated using ArcGIS.

Model Calibration

The BCM calculates the water balance in a series of steps. (1) The precipitation is determined to be rain or snow depending on air temperature. (2) Rain is added to the soil directly and snow is added directly or to the previous month's snowpack. (3) If a snow pack exists then snow loss is calculated as sublimation or snowmelt, again depending on temperature. (4) Rain or snowmelt then fills the available storage in the soil profile followed by removal of PET. (5) If the total amount of water in the soil profile exceeds the soil storage the excess water will become runoff. If the total amount of water in the soil profile is less than the soil storage but greater than field capacity it will be become recharge at a rate equivalent to the bulk bedrock permeability. (6) Any water remaining above field capacity is added to the runoff. (7) The soil water at or below field capacity is carried into the next month as soil water storage. To calibrate the model to measured streamflow all runoff and recharge upstream of a gage is summed and compared to the measured data. The calculated runoff is always routed to the gage and a proportion of recharge is added to the runoff as baseflow. Recharge then re-emerges into the river system as baseflow, and determining the proportion of recharge the re-emerges is part of the calibration process.

Calibration data

On the basis of analyses conducted by Saleh (2010) it was determined that four streamflow gages were available that were considered unimpaired, with no diversions or downstream dams, thus reflecting appropriate conditions for comparison to the BCM estimates of basin runoff. These gages are shown in table 1 with their locations, periods of record, elevation, and catchment area, and figures 2 and 8. Two

gages were located in large basins at the headwaters of the Euphrates River in Turkey, and two were in smaller basins in the headwaters of the Tigris River at the northern Iraq border with Turkey.

Calibration process

Calibration of the BCM is the iterative process of changing the Ksat to alter the proportion of water that becomes either runoff or recharge to better match streamflow. Ksat of the bedrock is increased to increase recharge and reduce runoff. Because the BCM is run at a monthly timestep, a recession function was added to the calibration procedure to allow for a better estimate of the fit. This is an exponent of between 0.8 and 0.92 that is added to the cumulative recharge value that results in a representation of baseflow to which runoff is added. Calibration results are illustrated in Figure 9 for each of the four gages. Given the uncertainties in the various components of the input parameters, (climate, geology, and soils data), the simulated volumes provide a reasonable match to the measured data for these four basins, with slight underestimates of peaks in the large basins in Turkey and slight overestimates of peaks in the smaller basins in Iraq.

Results and Discussion

The BCM was run for 1949-1999, the period of record with the most complete climatic records. Results are shown for monthly trends, annual time series, and average annual spatially distributed maps. Also included are volume estimates of recharge and runoff for all subbasins in the study area.

Regional water balance results

Monthly trends of climate and water balance parameters averaged for the entire study domain are shown in figure 11. Average annual air temperature follows the general Mediterranean climate with cold winters and hot summers (figure 11a). Maximum monthly air temperatures are about 10 to 18 degrees C higher than minimum monthly air temperatures, with the largest range in midsummer. The percentage of the total water balance that is represented for each month by snowfall, actual evapotranspiration, runoff, and recharge (figure 11b) shows that precipitation is the largest component in the winter, whereas evapotranspiration is the largest in the summer. Snowfall is present as a component from October through April, with the highest percentage in January, and recharge and runoff follow with a month lag. Recharge is larger than runoff for all months with the largest percentage in April. These trends follow similar patterns to many locations in the United States, particularly in California where the areas dominated by

snowfall and springtime snowmelt result in runoff and recharge, with the desert regions having small components of both runoff and recharge.

Average annual recharge is spatially distributed in figure 12, and supports the interpretation that recharge is located in regions with higher precipitation and particularly in areas with snowfall. Runoff shows similar patterns (figure 13) but is in less magnitude than recharge. These results are converted to volume, in millions of cubic meters per subbasin, in figures 14 and 15, providing a picture of the relative amounts of precipitation and resulting recharge and runoff in the TERS study area. Again, the majority of the precipitation is located in the mountains, particularly in the Tigris River basin, and while the majority of the recharge is in the headwaters of the Tigris, Euphrates, and Karun River basins, most is in the Tigris River basin. Runoff occurs predominantly in the headwaters of the Tigris, as well. Although precipitation occurs throughout the TERS with some snowfall occurring within about two-thirds of the area, because of the high evapotranspiration rates throughout the desert regions little to no recharge or runoff occurs in about half of the study area.

Average annual values of the water balance components are shown for the Tigris and Euphrates River basins as well as for each country within the TERS in table 3. To illustrate that the estimates in table 3 are within reasonable bounds, in the absence of reliable estimates of recharge, a comparison is made to an estimate of safe yield. Krasny and others (2006) estimate safe yield for the country of Iraq to be approximately 12,600 million cubic meters. Estimated recharge from the BCM was 7,000 million cubic meters and stream flow was 6,400 million cubic meters (table 3). Additional runoff generated from other countries was approximately 14,000 cubic meters. If 15 percent of the runoff from the Tigris and Euphrates Rivers becomes recharge to the groundwater system in Iraq (15 percent was used in the Great Basin according to Flint and Flint, 2007b), an additional 3,000 million cubic meters of recharge is added to the 7,000 for a total of 10,000 million cubic meters. In addition, it is likely that recharge in the mountains north and east of Iraq will contribute to groundwater recharge in Iraq through subsurface flow that would increase the estimate of recharge well above the 10,000 million cubic meters. This amount exceeds that of the estimate of safe yield by Krasny and others (2006), and it is recognized that the two properties are not equivalent, safe yield should be a percentage of recharge.

The majority of precipitation falls in the Tigris River basin, over twice that of the Euphrates River basin, yet the Euphrates has the most loss to potential evapotranspiration. The Tigris River basin also receives the most snowfall, and results in about 30 percent more recharge and 3 times more runoff than the Euphrates. The majority of the precipitation and resulting recharge and runoff are in Turkey. More

precipitation falls in Iraq than in Syria, Iran, or Saudi Arabia, and more results in runoff, although less of it results in recharge than in Iran. Within the TERS, Saudi Arabia has little precipitation and no recharge or runoff.

Changing climate in the Tigris Euphrates River System

Future projections of climate in the Middle East are extremely variable. Simulating the climate of the region is a challenge for climate models, due in part to the high natural inter-annual variability, the topography of the region - which includes multiple mountain ranges and inland seas (Hemming and others, 2010; Evans, 2009). Recent projections from the Intergovernmental Panel on Climate Change (IPCC) raised fears that storm activity in the eastern Mediterranean would decline this century if global warming continues on present trends. In turn, that would have reduced rainfall by between 15 and 25 per cent over a large part of the land encompassing parts of Turkey, Syria, northern Iraq, and north-eastern Iran and the strategically important headwaters of the Tigris and Euphrates rivers. However, the IPCC report compared model results from 12 different models using one emission scenario and found that for much of Iraq, less than two-thirds of the models agreed whether more or less precipitation would occur. Recent research done by the University of New South Wales Climate Change Research Centre (Evans, 2009) suggests that these projections would result in significant challenges to the region's agricultural base, with a longer dry season and changes in the timing of maximum rainfall. However, the researcher notes that the IPCC projections were based on the results of global modeling of climate change, which tends to obscure smaller-scale regional effects. As a follow up study, Evans used regional climate modeling specific to the Middle East, with results that suggest, despite declines in storm activity, that moisture-bearing winds would be channeled inland more often and diverted by the Zagros Mountains, bringing an increase of over 50 percent in annual rainfall to the Euphrates-Tigris watershed (Evans and Smith, 2010). With these widely ranging projections and interpretations that depict future Middle Eastern climatic conditions, the use of currently measured conditions and trends serves to lay a foundation for forecasting ongoing changes in climate and hydrology.

Changes in climate are ongoing worldwide and evidence suggests that climate changes in the Middle East over the last several decades may have been a result of global warming. To illustrate some slight changes in the climate and resulting recharge and runoff, the water balance results are illustrated as annual time series for 1949-1999 for both the Tigris and Euphrates River basins (figures 16 and 17). A slight downward trend is apparent in precipitation for both basins (figure 16a), while slight increases can be seen in potential evapotranspiration (figure 16b) and air temperature (figure 16c). These are translated

into a larger decrease in snowfall over the 50 year period (figure 17a), and a less noticeable decline in recharge and runoff (figure 17 b and c). More significant trends can be seen over the last 30 years.

The 50-year time period for which these analyses were done encompasses the time frames within which large scale climatic cycles occur, most notably the North Atlantic Oscillation (NAO), a dominant mode of Atlantic sector climate variability, and the Arctic Oscillation, both of which generally vary on decadal time scales. Positive phases of these indices bring drier conditions to the Middle East, while negative phases are generally wetter. Generally, since the end of the 1980s, both indices have been systematically positive, coinciding with relatively warm conditions (Cullen and others, 2002). Interannual to decadal changes in December through March precipitation and streamflow in the eastern Mediterranean are tied to the NAO (Cullen and others, 2002; Eshel and Farrell, 2000). Over the past several decades, the NAO index has steadily strengthened, rising from its low index state in the 1960s to a historic maximum in the 1990s. This trend accounts for a significant portion of the winter temperature increase over Eurasia (Hurrell and Van Loon, 1997; Hurrell and others, 2001).

This trend is apparent in the temperature and evapotranspiration data shown in figures 16 b and c, and the decline of BCM-simulated recharge and runoff throughout the 90s (figure 17 b and c). Additionally, links have been established between changes in Middle Eastern water supply associated with natural variations in the climate system and sea surface temperature variations in the Atlantic Ocean and eastern Mediterranean Sea. These links suggest that if the NAO, influenced by increased greenhouse gases, continues its upward trend, then future amounts of December through March precipitation and streamflow can be expected to be lower (Cullen and others, 2002).

The spatial variation in how the water balance changes over time within a region may indicate locations that are more or less sensitive to changes in climate, for reasons such as topographic influences on climate resulting in localized refugia, or regional influences on climatic patterns, or elevational gradients. An analysis was done of climatic data that evaluated the trend in climate and hydrology over the 50-yr period 1949-1999 by developing regressions of 50 yearly values for every 180-m gridcell, resulting in the spatially distributed change in the value over the time period. This is shown for snowfall, encompassing most of the changes in precipitation and air temperature, in figure 18. This illustrates an increase over the 50-yr period at the highest elevations in the TERS in Turkey, at the headwaters of both the Tigris and Euphrates rivers. All other locations have declined in snowfall. Corresponding changes in recharge for this period are shown in figure 19 and illustrate the differences in recharge in higher elevation areas that have snow from those that do not. There is evidence in regions with warm snowpack that the highest

elevation locations may be receiving increases in moisture with warming climates that are being translated into increases in snow at elevations that are still below freezing in the winter. As a result, and despite the increases in potential evapotranspiration, there are increases in recharge in these regions. This is more pronounced in the Euphrates River basin than the Tigris, however, whereas the increases in runoff that have occurred over the 50-yr period are centered over the location with increases in snowfall. There are also differences in northern Iraq where recharge has been increasing and runoff has been declining, as well as in the Karun River basin. The change in snowfall and subsequent springtime snowmelt causes changes in the timing of runoff, and rain on snow events that cause increases in peak flows. Decreases in snowpack, such as in the northwestern portion of the Euphrates River basin, may provide the opportunity for recharge to occur during the winter when evapotranspiration is low, whereas runoff occurs more predominantly as a function of snowmelt.

Summary and Conclusions

To support and encourage economic development and stability in Iraq, scientists with the U.S. Geological Survey are providing information, expertise, and technological assistance in regard to Iraq's water resources, and creating the necessary infrastructure to enable easy access and sharing of national geospatial data. As part of this endeavor, the unimpaired flows in the Tigris and Euphrates Rivers have been assessed using regional water balance modeling to provide an understanding of the historical hydrologic conditions, how they are currently changing, and to provide the basis for evaluating the effects of upstream development on Iraq’s current and projected surface water supplies.

Regional water balance modeling was applied to the Tigris Euphrates River system, necessitating the development and downscaling of mostly global datasets for this data poor region. Transient climate data obtained from coarse scale CRU datasets, interpolated and scaled to fine scale monthly average WorldClim patterns, were downscaled further for model application at 180-m spatial resolution. Very coarsely mapped soils data was further developed to reflect fine scale geomorphic and topographic features. Geologic maps of the region were combined and interpreted to provide a starting point for model calibration. The model, calibrated to four available unimpaired streamflow records, was then applied to the region to establish a monthly hydrologic record for 1949-1999.

Results of the Basin Characterization Model for 1949-1999 illustrate the importance of snowfall to recharge and runoff in the TERS, with the majority of recharge and runoff in the mountainous regions

where snow occurs. The decline of snowfall over the 50-yr period is apparent, but these preliminary results suggest inconclusively that runoff is being impacted more by the decline in snowfall than in recharge.

The Tigris River basin receives the majority of precipitation and the least potential evapotranspiration, resulting in 30 percent more recharge and three times more runoff. Although a more rigorous analysis that includes the last 10 years of record (1999-2009) is warranted, climate changes over the past few decades are translating into slight changes in hydrology. These are illustrated as declines in precipitation and increases in potential evapotranspiration and air temperature, resulting n decreases in snow. These trends are more obvious since the late 1980s. The spatial distribution of how the water balance has changed over the 50-yr period illustrates that although snowfall has declined over the region, locations with the highest elevations have had increases in snow and thus increases in recharge and runoff. These trends have implications for shorter term management considerations.

References

Adnan, A., Domas, J., and Jassim, S.Z., 2006, Quaternary Deposits: Chapter 15 in Geology of Iraq, S. Z. Jassim and J. C.Goff. (eds), Dolin, Hlavni Publishers, Brno, Czech Republic, p.185 – 198.

Allen, R.G., Pereira, L.S., Raes, D., 1998, Crop evapotranspiration-Guidelines for computing crop water requirements: FAO Irrigation and drainage paper 56, Rome, Italy, 300 p.

Bear, J., Shamir, U., and Hefez, E.A., 1972, Numerical modeling of groundwater systems: Technion-Israel Institute of Technology, 76 p.

Buringh, P., 1960, Soils and Soil Conditions in Iraq: Ministry of Agriculture, Baghdad, Iraq, 214 p. http://library.wur.nl/isric/index2.html?url=http://library.wur.nl/WebQuery/isric/648

Cullen, H.M., Kaplan, A., Arkin, P.A., and Demenocal, P.B., 2002, Impact of the north Atlantic oscillation on middle eastern climate and streamflow: Climatic Change 55:315-338.

Eshel, G., Farrell, C. M., and Farrell, B., 2000, Forecasting eastern Mediterranean droughts: Mon. Weather Rev. 128:3618–3630.

Evans, J.P., 2009, 21st century climate change in the Middle East: Climatic Change 92:417-432.

Evans, J. P., and Smith, R.B., 2006, Water vapor transport and the production of precipitation in the eastern Fertile Crescent: J. Hydrometeor, 7, 1295–1307.

FAO/IIASA/ISRIC/ISS-CAS/JRC, 2009. Harmonized World Soil Database (version 1.1). FAO, Rome, Italy and IIASA, Laxenburg, Austria.
http://www.iiasa.ac.at/Research/LUC/External-World-soil-database/HTML/index.html?sb=1

Flint, A.L., Flint, L.E., Hevesi, J.A., and Blainey, J.M., 2004, Fundamental concepts of recharge in the Desert Southwest: a regional modeling perspective, in Groundwater Recharge in a Desert Environment: The Southwestern United States, edited by J.F. Hogan, F.M. Phillips, and B.R. Scanlon, Water Science and Applications Series, vol. 9, American Geophysical Union, Washington, D.C., 159-184.

Flint, L.E., and Flint, A.L., 2007a, Regional analysis of ground-water recharge, in Stonestrom, D.A., Constantz, J., Ferré, T.P.A., and Leake, S.A., eds., Ground-water recharge in the arid and semiarid southwestern United States: U.S. Geological Survey Professional Paper 1703, p. 29-59.

Flint, A.L., and Flint, L.E., 2007b, Application of the basin characterization model to estimate in-place recharge and runoff potential in the Basin and Range carbonate-rock aquifer system, White Pine County, Nevada, and adjacent areas in Nevada and Utah: U.S. Geological Survey Scientific Investigations Report 2007-5099, 20 p.

Flint, L.E., and Flint, A.L., Downscaling future climate scenarios to fine scales for hydrologic and ecologic modeling and analysis. (In review)

Freeze, R.A., and Cherry, J.A., 1979, Groundwater: Prentice-Hall, 604 p.

GEOSURV, 2000, Geological map of Iraq, 1:1,000,000: 3rd revision, State Company of Geological Survey and Mining, Baghdad.

Hemming, D., Buontempo, C., Burke, E., Collins, M, and Kaye, N., 2010, How uncertain are climate model projections of water availability indicators across the Middle East?: Phil. Trans. R. Soc. A, 368(1931): 5117-5135.

Hijmans, R.J., Cameron, S.E., Parra, J.L., Jones, P.G., and Jarvis, A., 2005 Very high resolution interpolated climate surfaces for global land areas: Int. J. of Climatology 25:1965-1978.

Hurrell, J. and Van Loon, H., 1997, Decadal variations in climate associated with the North Atlantic Oscillation: Climatic Change 36:301–326.

Hurrell, J., Kushnir, Y., and Visbeck, M., 2001, The North Atlantic Oscillation: Science 291:603–605.

Jassim, S.Z. and Al-Gailani, M., 2006, Hydrocarbons: Chapter 18 in Geology of Iraq, S. Z. Jassim and Buday, T. (eds), Dolin, Hlavni Publishers, Brno, Czech Republic, p. 232-249.

Jassim, S. Z., and Goff, J.C., 2006, Phanerozoic development of the northern Arabian Plate: Chapter 3 in Geology of Iraq, S. Z. Jassim and Buday, T. (eds), Dolin, Hlavni Publishers, Brno, Czech Republic, p. 32-44.

Krasny, J., Alsam, S., and Jassim, S.Z., 2006, Hydrogeology: Chapter 19 in Geology of Iraq, S. Z. Jassim and Buday, T. (eds), Dolin, Hlavni Publishers, Brno, Czech Republic, p. 251 – 287.

Lees, G.M. and Falcon, N. L., 1952, The geographical history of the Mesopotamian Plains: The Geographical Journal, 118(1): 24-39. http://www.jstor.org/stable/1791234

Metz, H.C. (ed.), 1988, Iraq: A Country Study: Washington, GPO for the Library of Congress.

Mitchell, T.D., and Jones, P.D., 2005, An improved method of constructing a database of monthly climate observations and associated high-resolution grids: Int. J. Climatology 25:693-712.

Nalder, I.A., and Wein, R.W., 1998, Spatial interpolation of climatic normals, test of a new method in the Canadian boreal forest: Agricultural and Forest Meteorology 92: 211– 225.

Pawlewicz, M.J., Steinshouer, D.W., and Gautier, D.L., 2003, Map showing geology, oil and gas fields, and geologic provinces of Europe including Turkey: U.S. Geological Survey Open File Report 97-470I, one CD-ROM.

http://pubs.usgs.gov/of/1997/ofr-97-470/OF97-470I/

Pollastro R.M., Karshbaum A.S, and Viger R.J., 1999a, Map showing geology, oil and gas fields, and geologic provinces of the Arabian peninsula: U.S. Geological Survey Open File Report 97-470B, one CD-ROM. http://pubs.usgs.gov/of/1997/ofr-97-470/OF97-470B/

Pollastro R.M., Persits, F.M., Steinhouer, D.W., 1999b, Map showing geology, oil and gas fields, and geologic provinces of Iran: U.S. Geological Survey Open File Report 97-470G, one CD-ROM. http://pubs.usgs.gov/of/1997/ofr-97-470/OF97-470G/

Saleh, D.K., 2010, Stream gage descriptions and streamflow statistics for sites in the Tigris River and Euphrates River Basins, Iraq: U.S. Geological Survey Data Series 540, 146 p.

Schaap, M.G., Leij, F.J., van Genuchten, MTh., 2001. Rosetta: a computer program for estimating soil hydraulic parameters with hierarchical pedotransfer functions: J. Hydro. 251, 163-176. http://www.ussl.ars.usda.gov/models/rosetta/rosetta.HTM

Shuttleworth, W.J., 1993, Evaporation: Chapter 4 in Maidment, D.R. (ed.), Handbook of Hydrology: New York, McGraw-Hill, 53 p.

van Genuchten, M.Th., 1980, A closed-form equation for predicting the hydraulic conductivity of unsaturated soils: Soil Sci. Am. J. 44:p. 892-898.

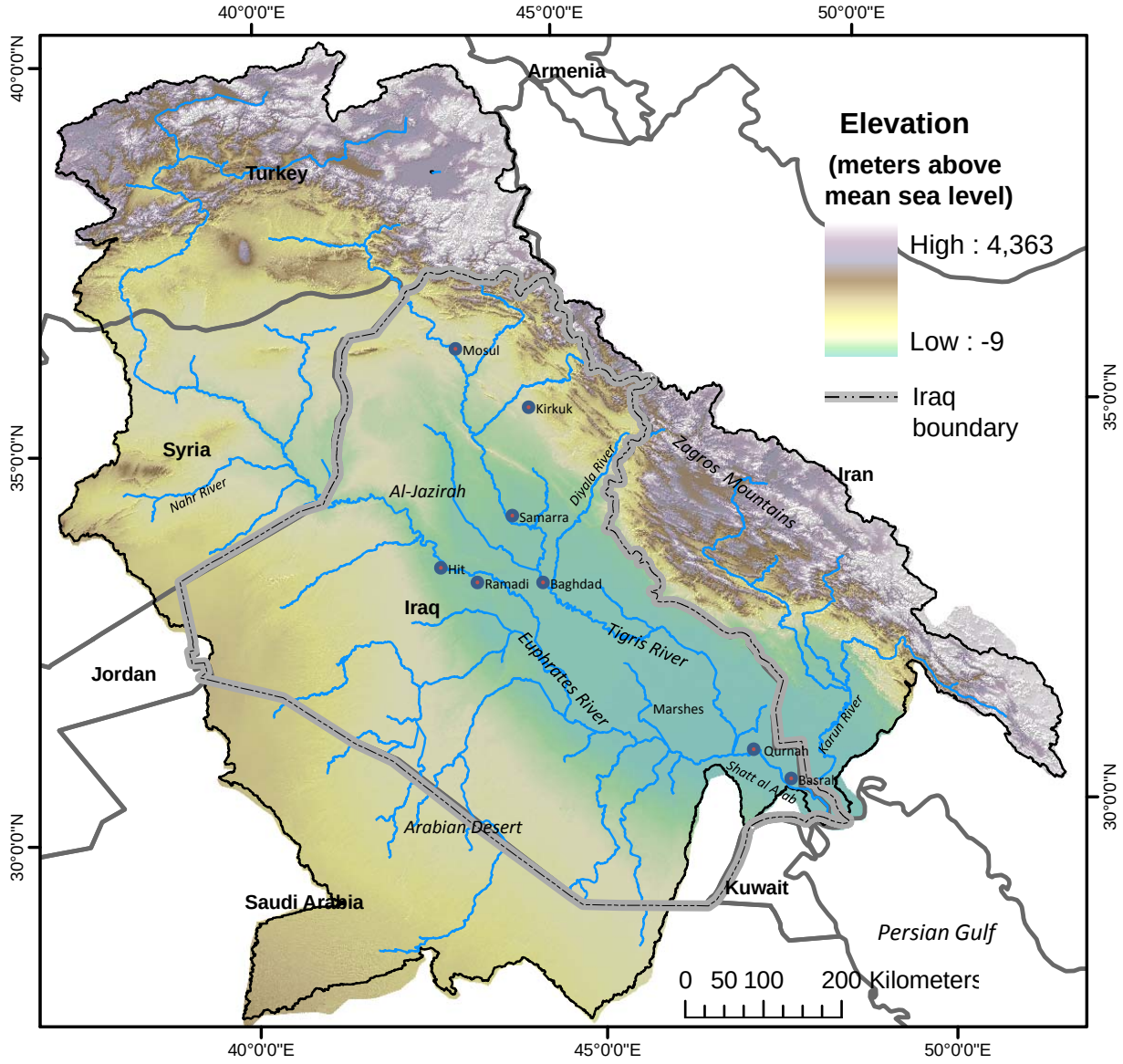

Figure 1. Map of Tigris Euphrates River System, including country boundaries and elevation.

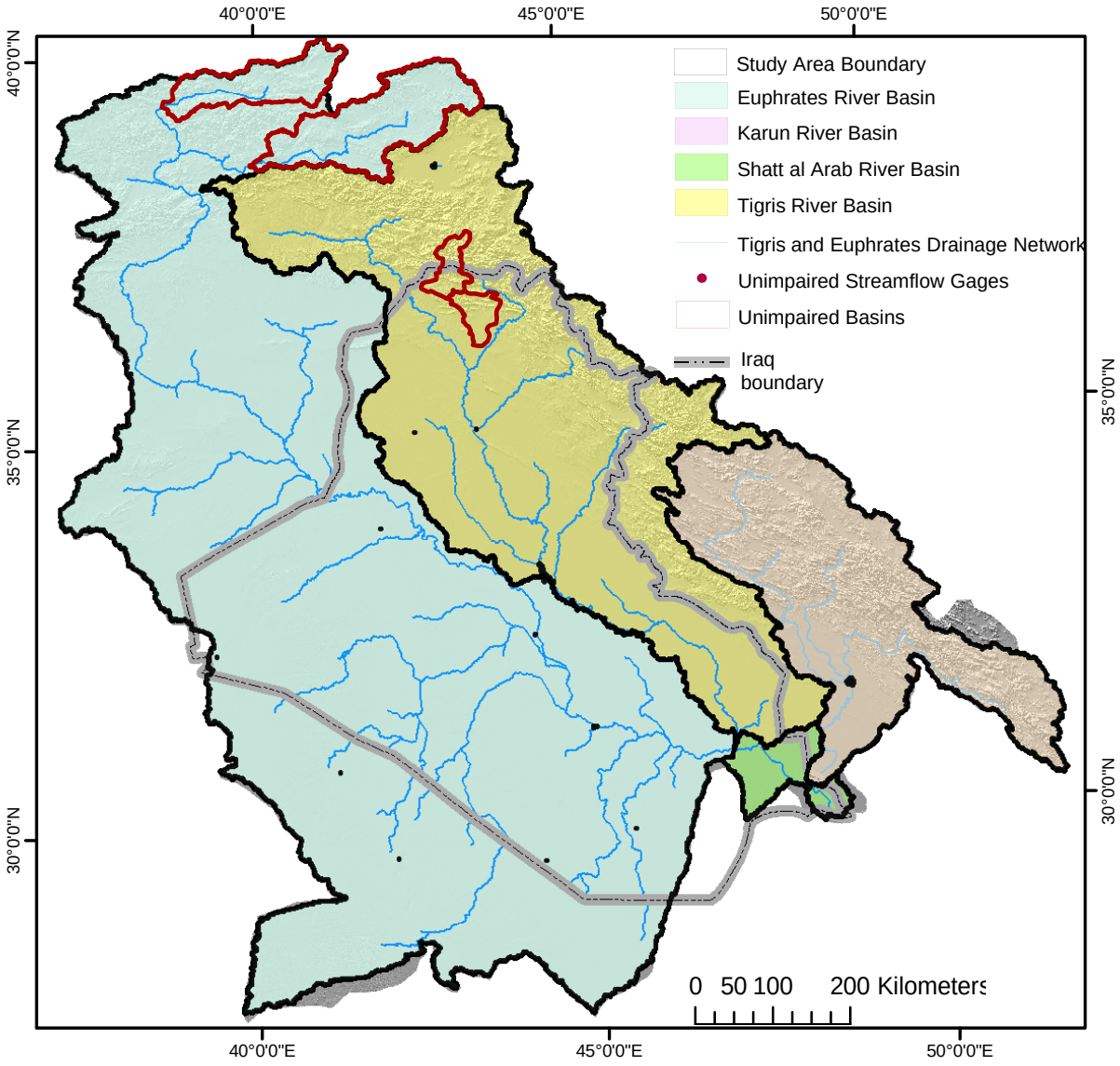

Figure 2. Map of Tigris Euphrates River System (TERS), study area boundary, major river basins and subbasins, calibration basins, and unimpaired streamflow gages.

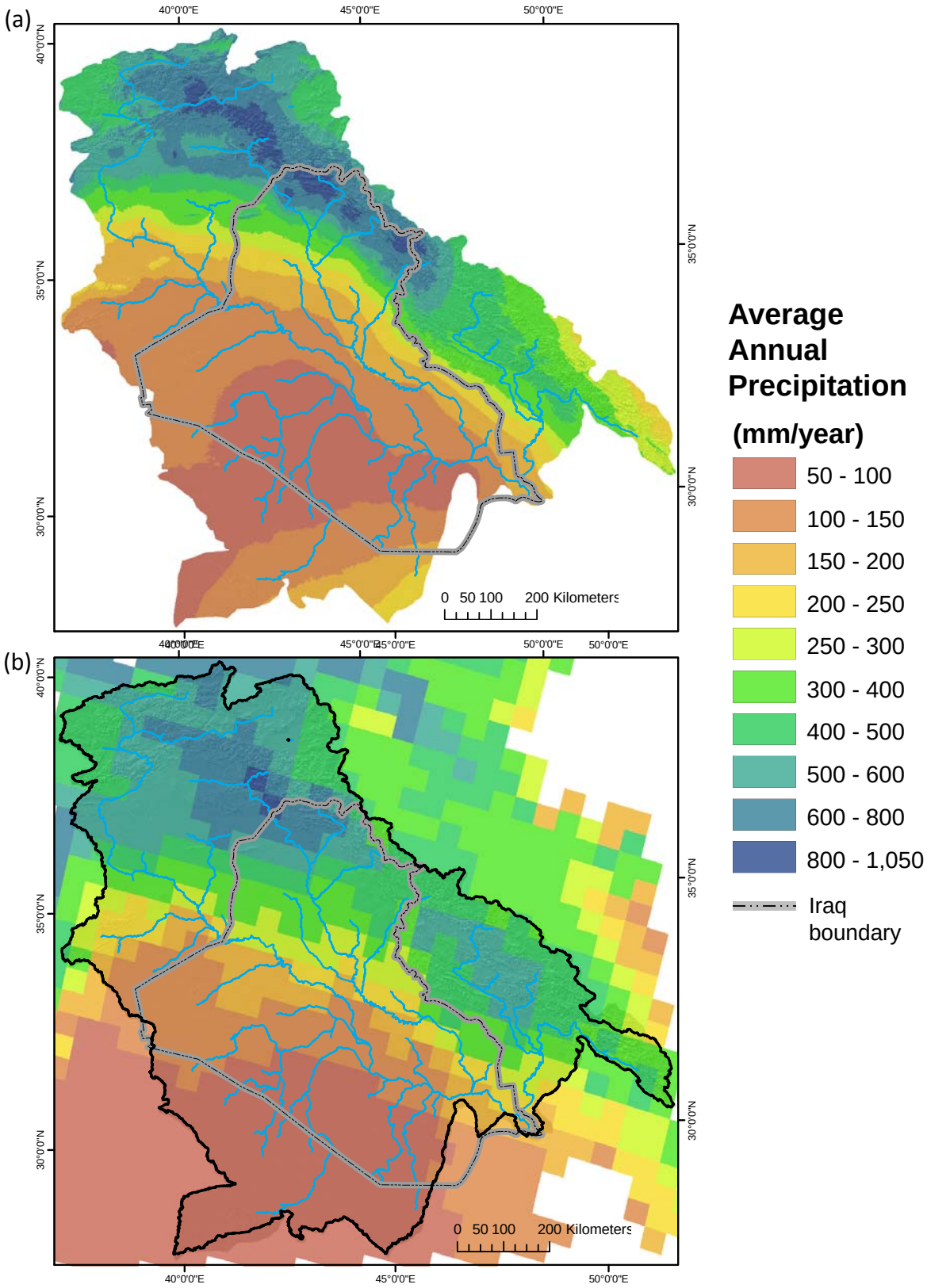

Figure 3. Map of average annual precipitation for the Tigris Euphrates River System at (a) 180-m spatial resolution used for Basin Characterization Model, and (b) original spatial resolution of 51.6 km from data available from the Climatic Research Unit (University of East Anglia, Norwich, UK; http://www.cru.uea.ac.uk/cru/data/hrg/).

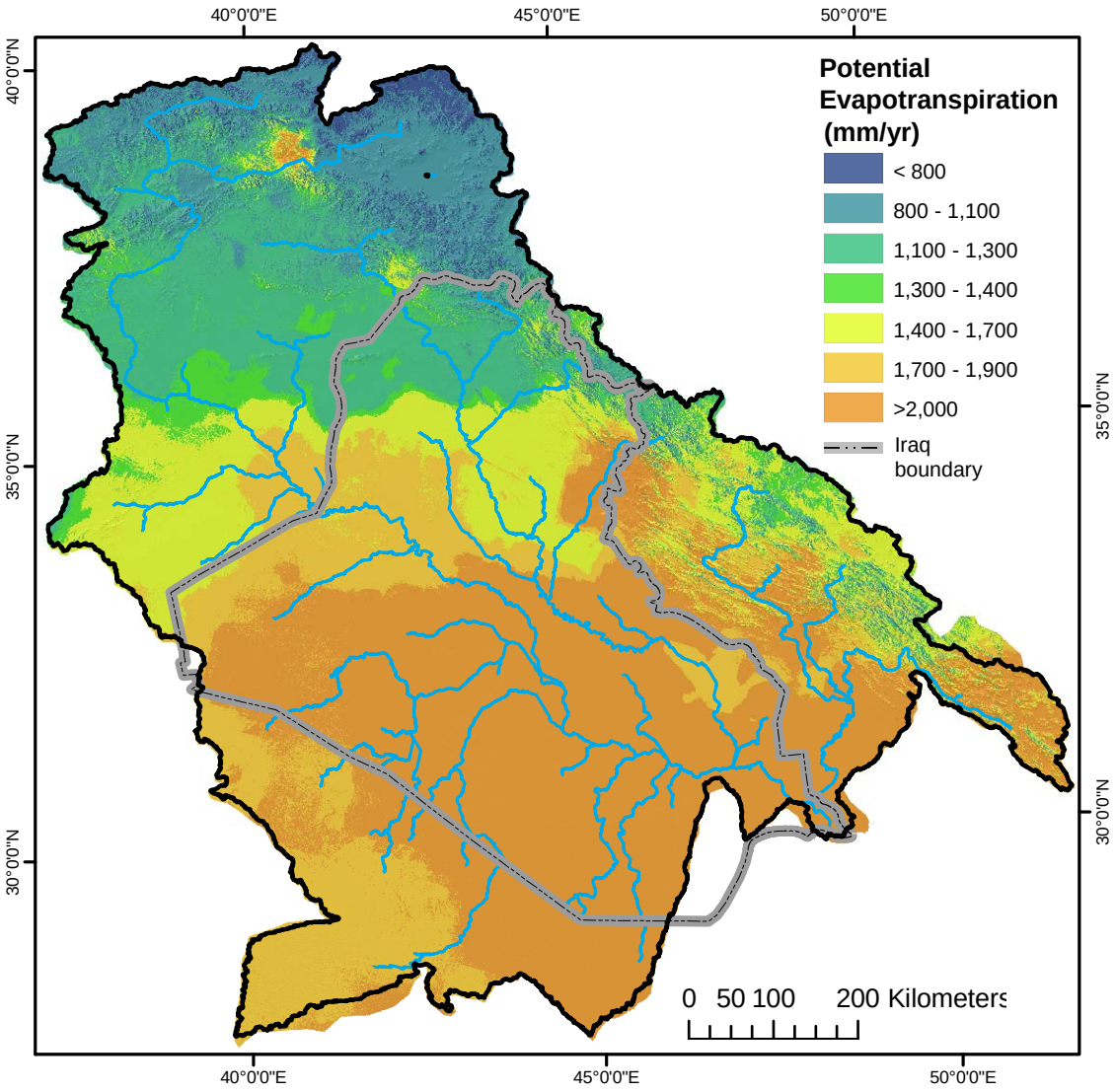

Figure 4. Map of annual potential evapotranspiration for the Tigris Euphrates River System (USGS Early Warning and Environmental Monitoring Program; http://earlywarning.usgs.gov/fews/middleeast/index.php).

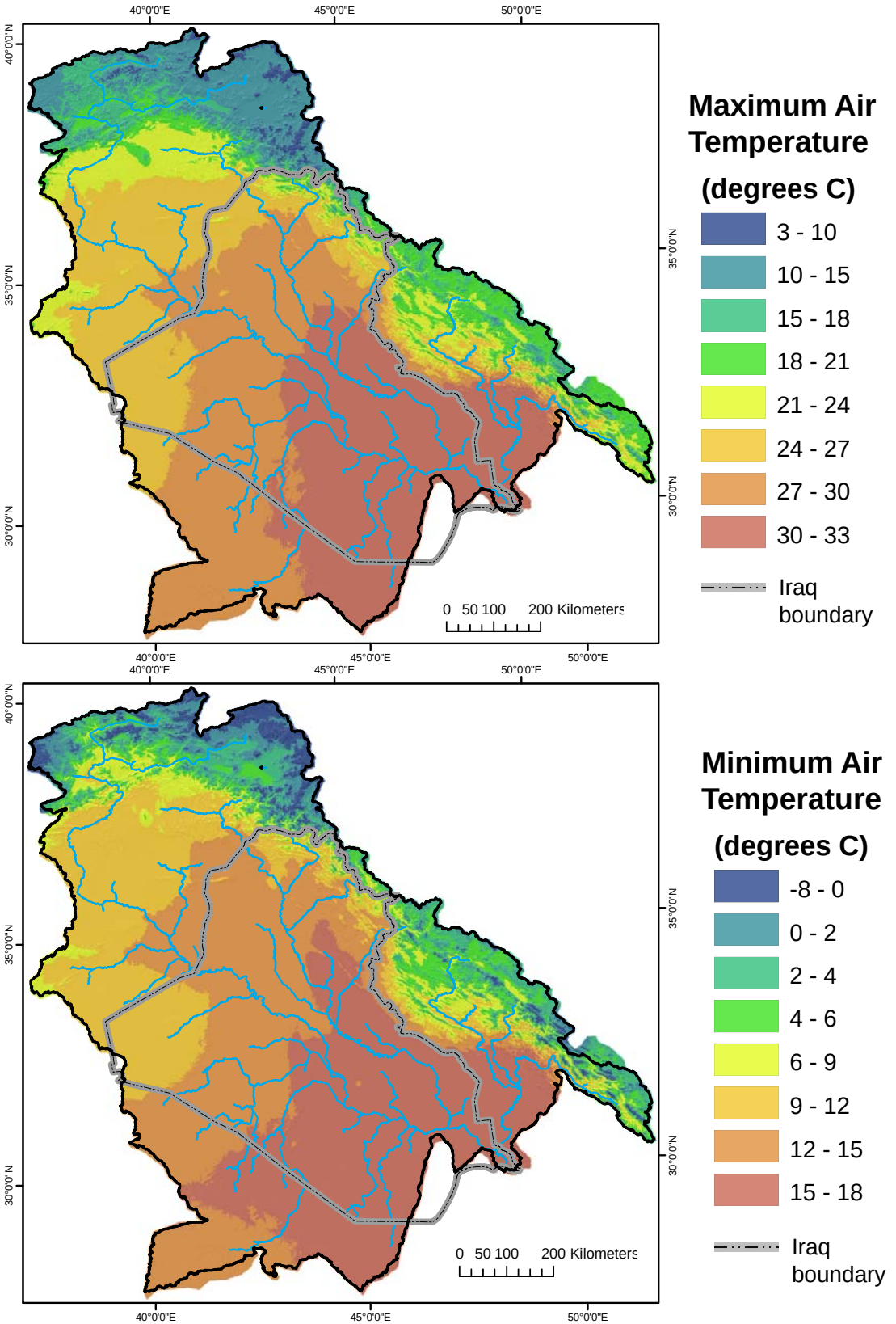

Figure 5. Map of average annual maximum and minimum air temperature for the Tigris Euphrates River System (Hijmans and others, 2005; http://worldclim.org/).

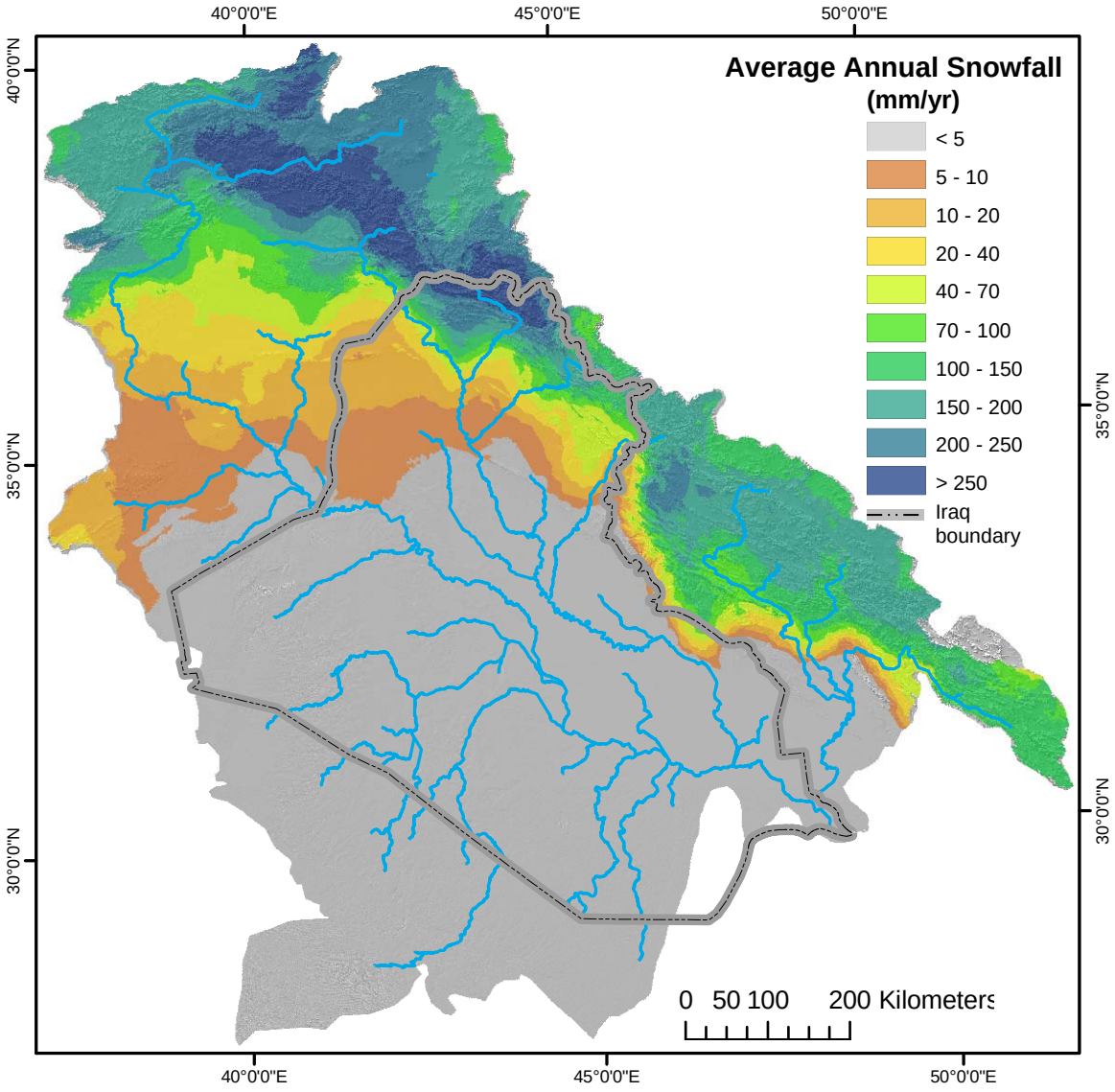

Figure 6. Map of average annual snowfall for the Tigris Euphrates River System . Snowfall is calculated from air temperature and precipitation data (Hijmans and others, 2005; http://worldclim.org/) using the Basin Characterization Model (Flint and Flint, 2007a).

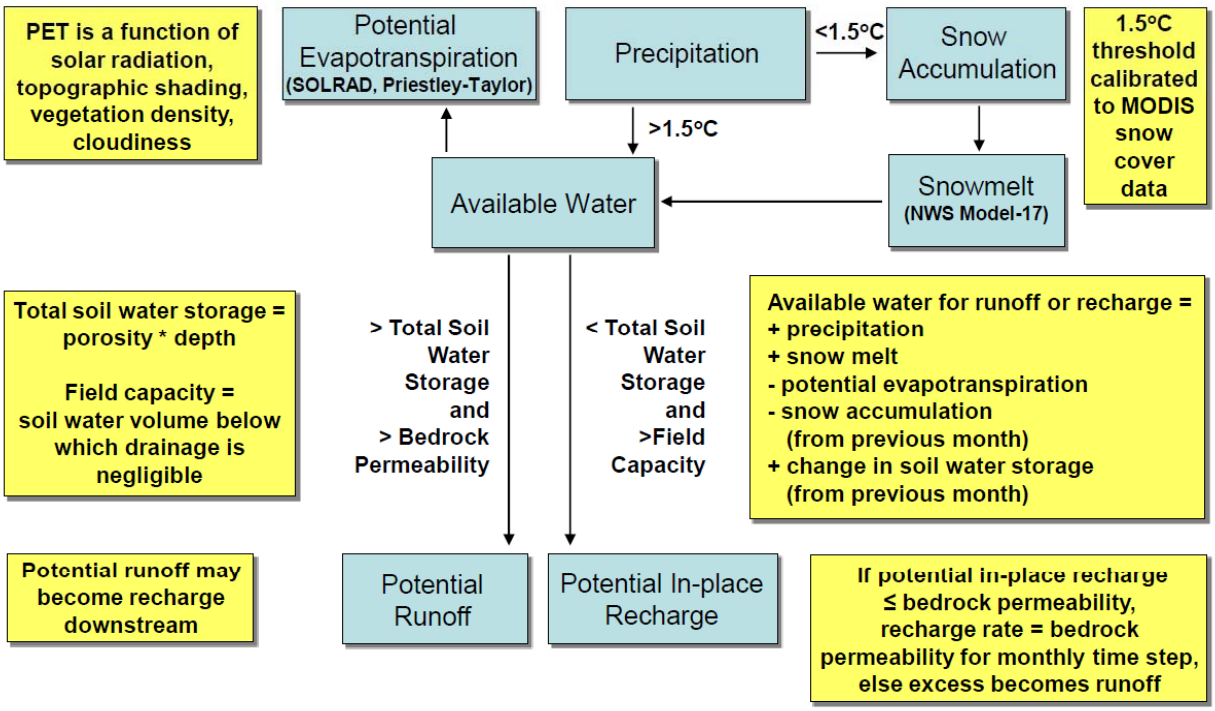

Figure 7. Schematic of the Basin Characterization Model indicating components of the monthly water balance, decision points, and how runoff and recharge are calculated.

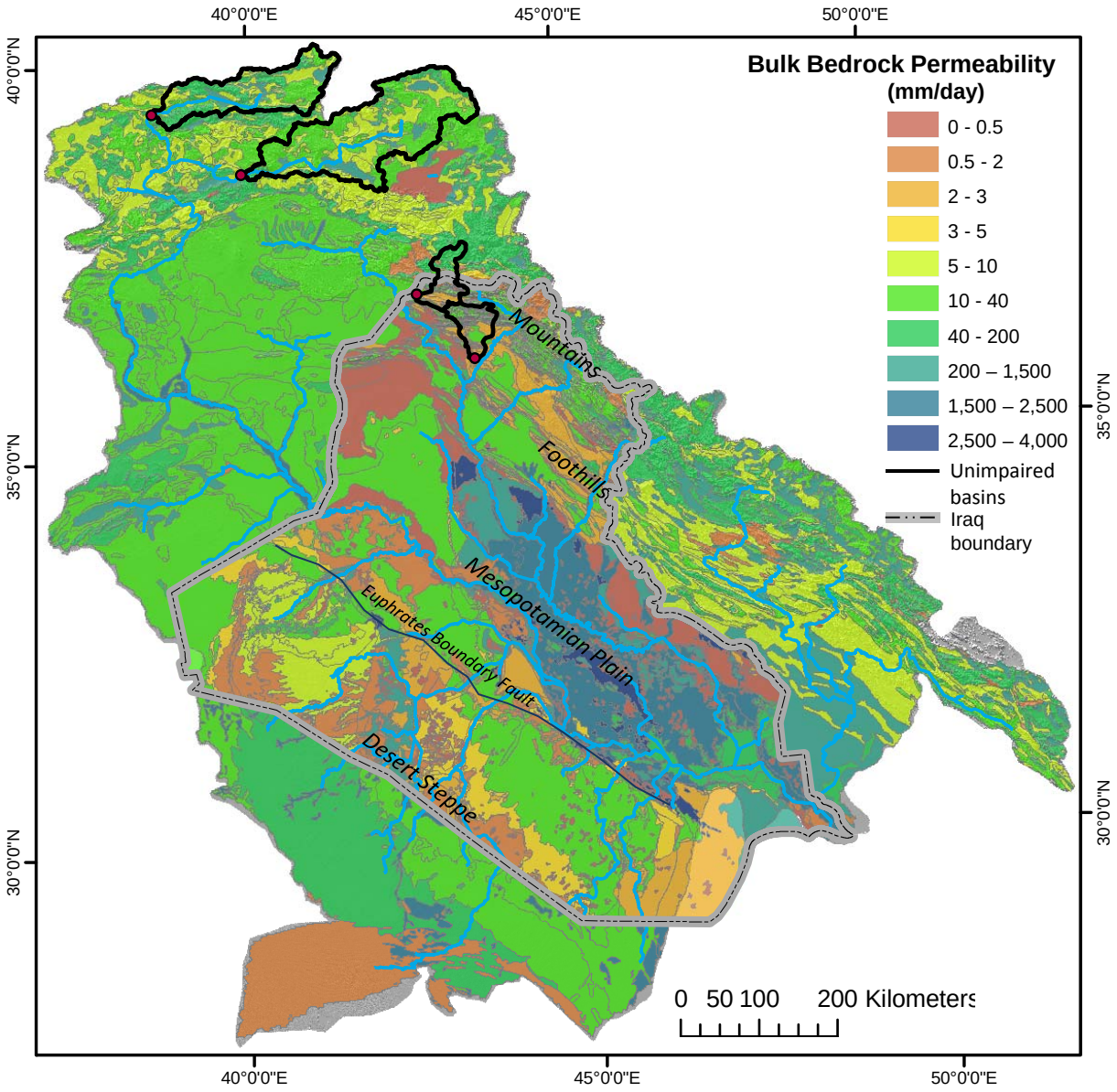

Figure 8. Map of surficial saturated hydraulic conductivity derived from geology for the Tigris Euphrates River System. Geomorphic providences are included.

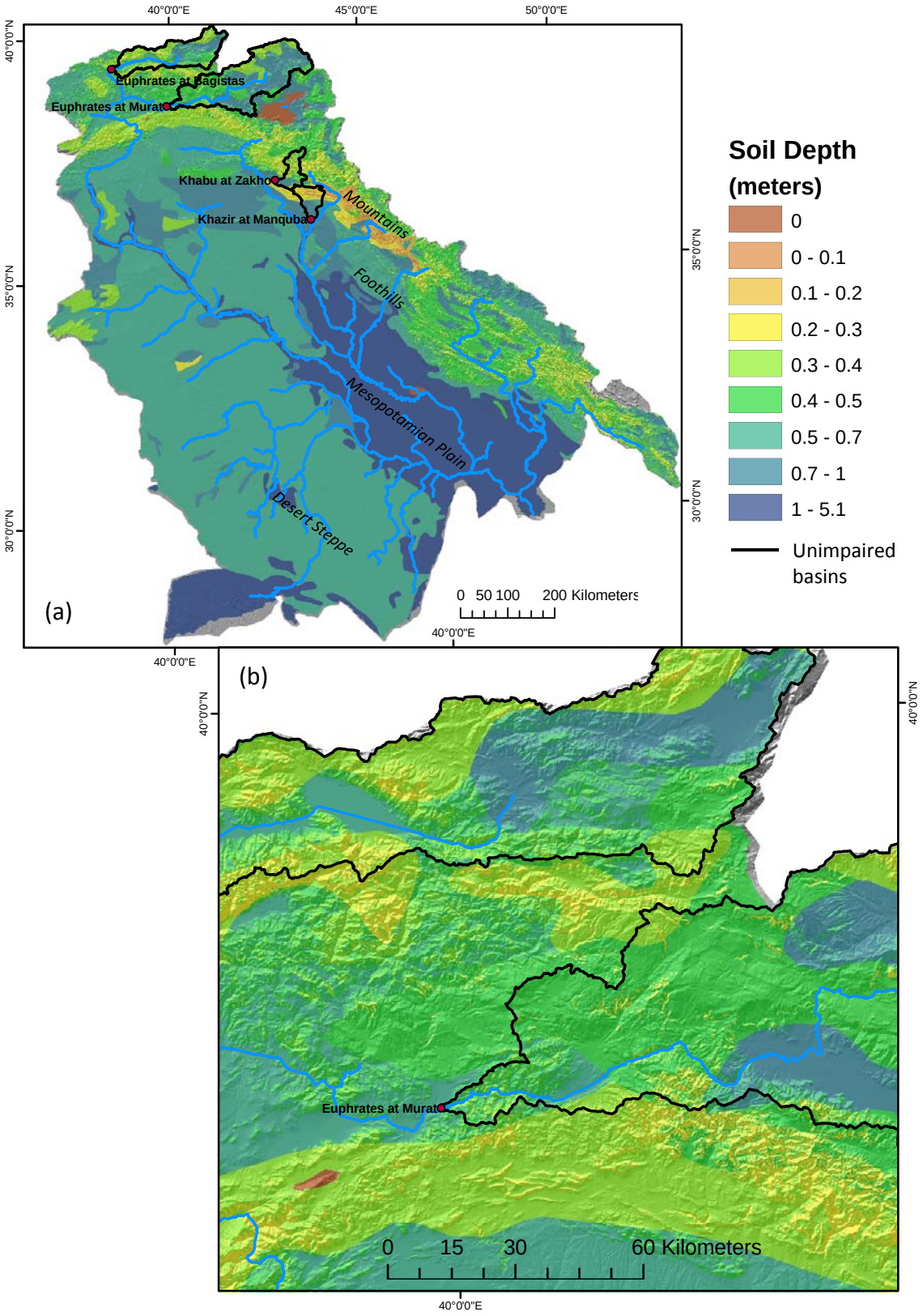

Figure 9. Map of soil depth developed for (a) the Tigris Euphrates River System and (b) a close up illustrating the impact of slopes on derived soil depth.

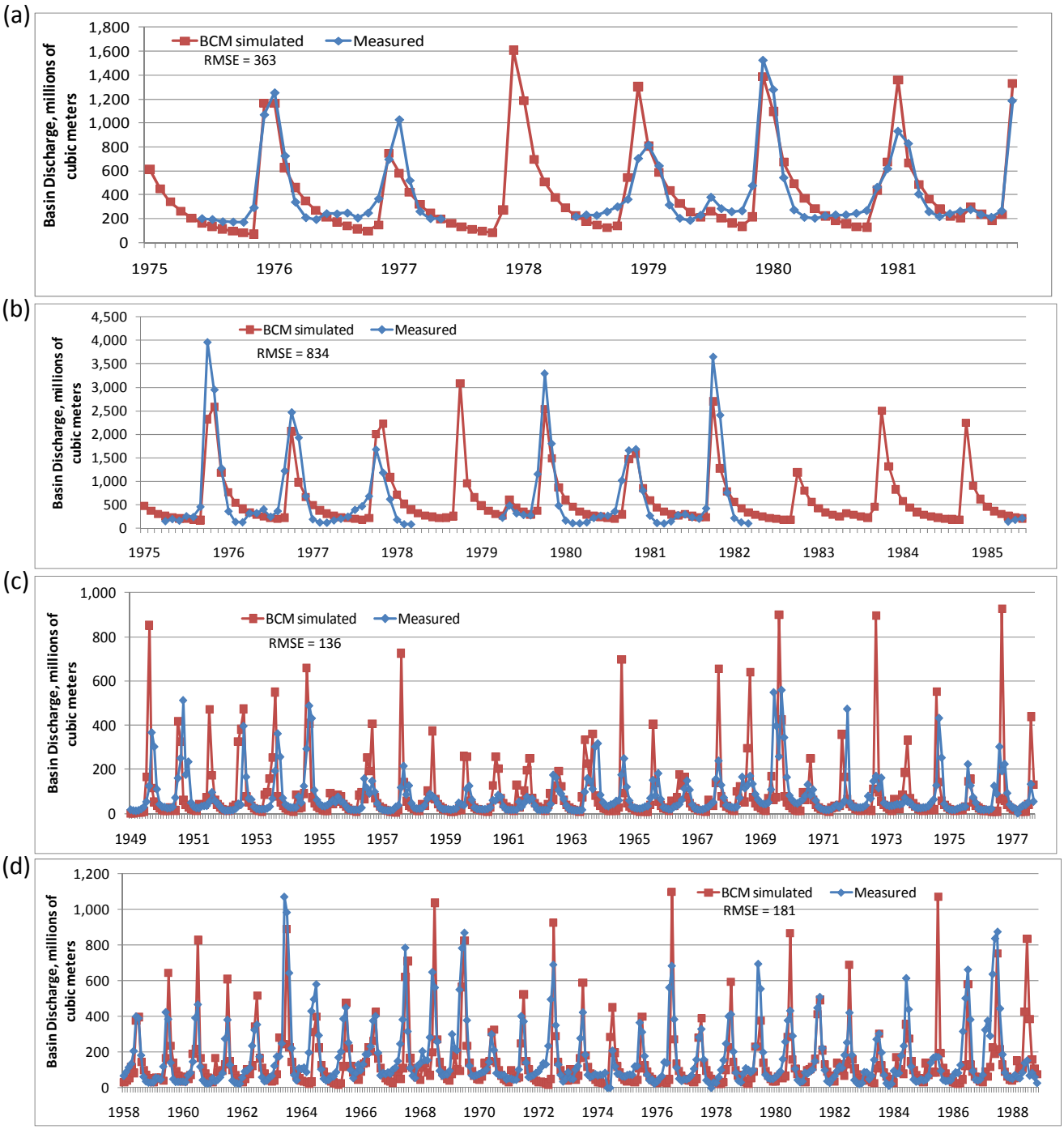

Figure 10. Calibration results comparing simulated and measured basin discharge for stramflow gages at (a) Euphrates at Bagistas, (b) Euphrates at Murat, (c) Khazir at Manquba, and (d) Khabu at Zahko, for the period of record for each gage.

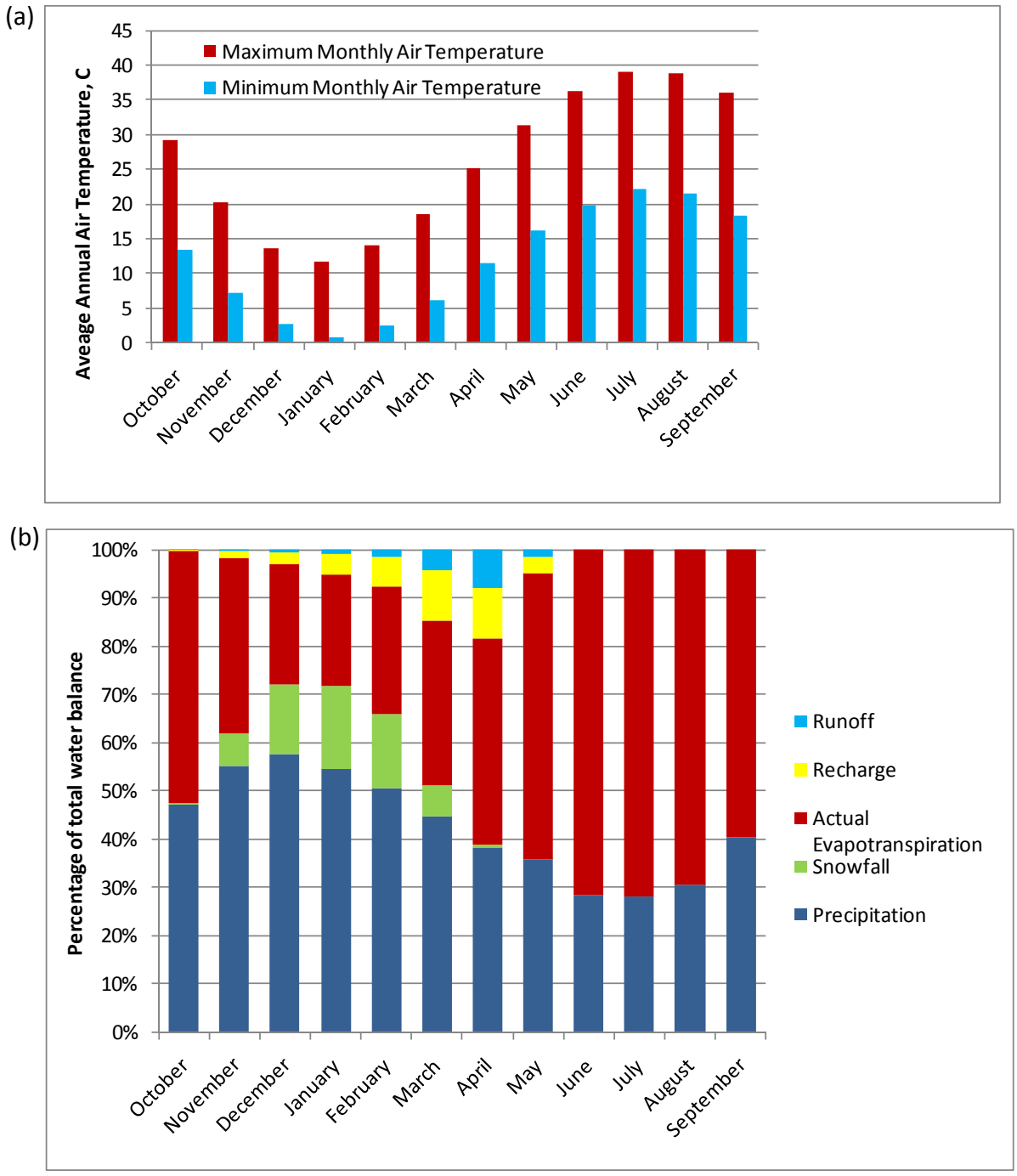

Figure 11. Average monthly (a) air temperature and (b) Basin Characterization Model results of water balance components depicted as the percentage of the total water balance.

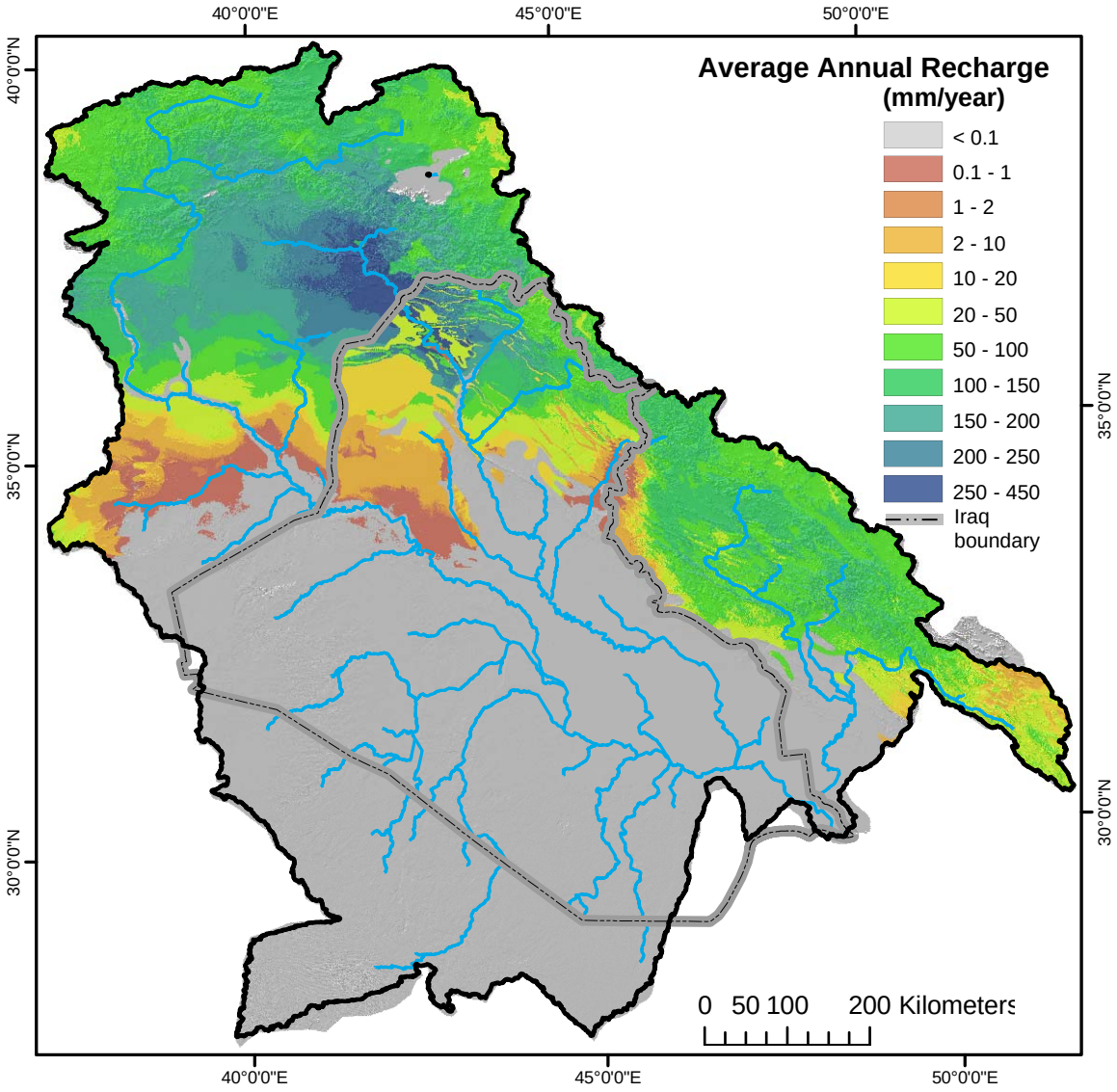

Figure 12. Map of average recharge for 1949-1999 for the Tigris Euphrates River System using the Basin Characterization Model.

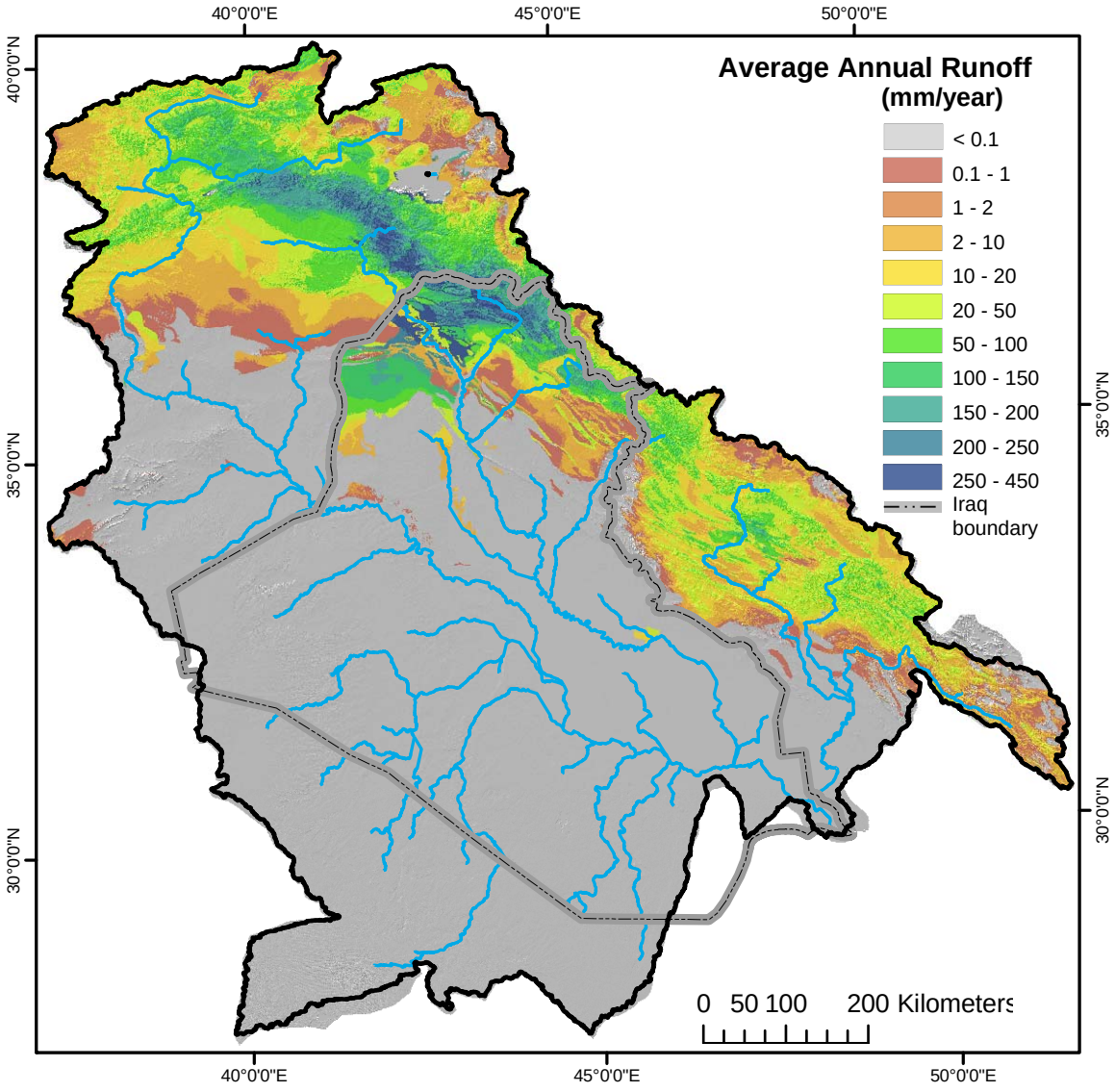

Figure 13. Map of average annual runoff for 1949-1999 for the Tigris Euphrates River System using the Basin Characterization Model.

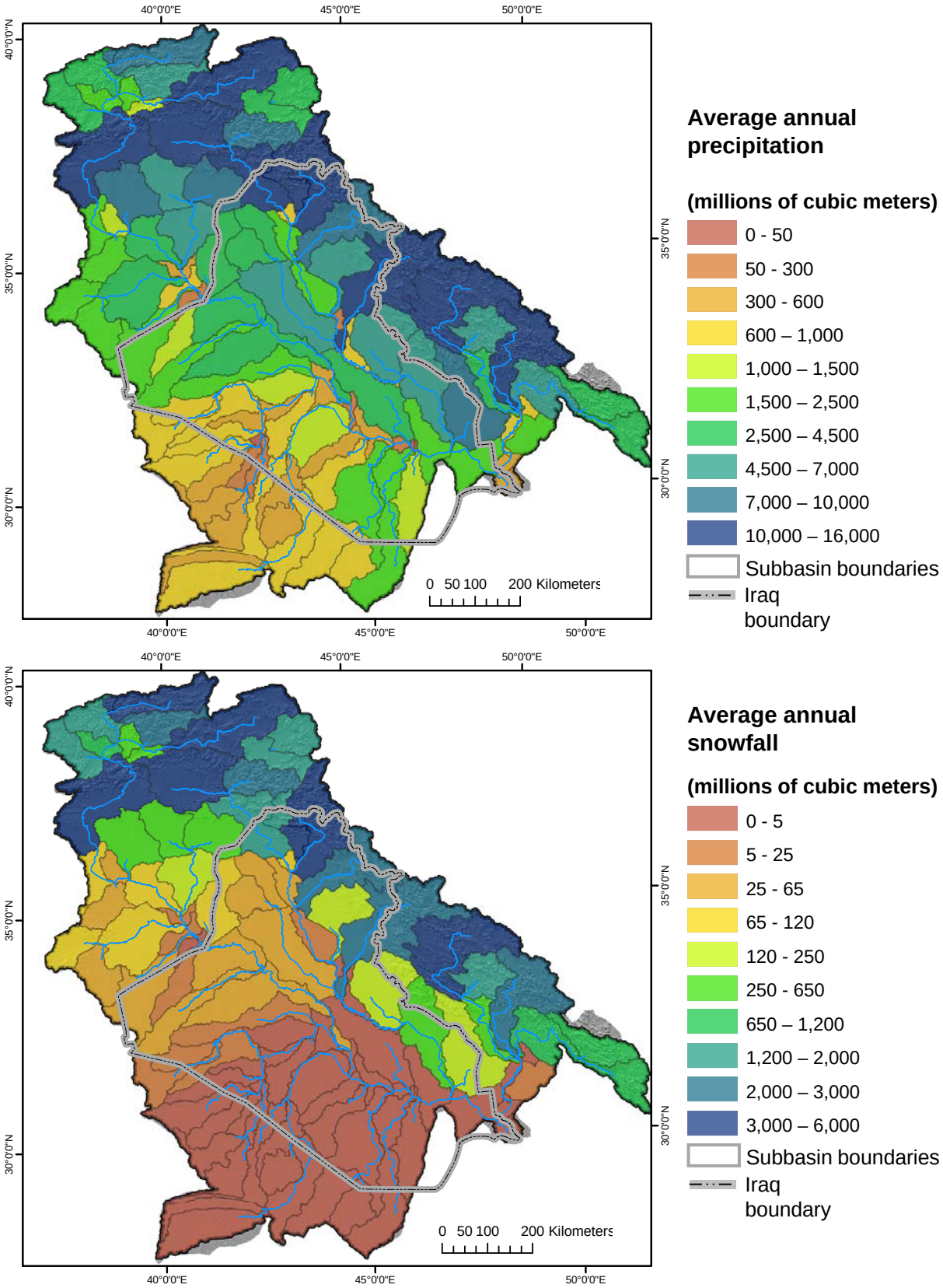

Figure 14. Maps of average annual precipitation and snowfall as volumes for each subbasin in the Tigris Euphrates River system.

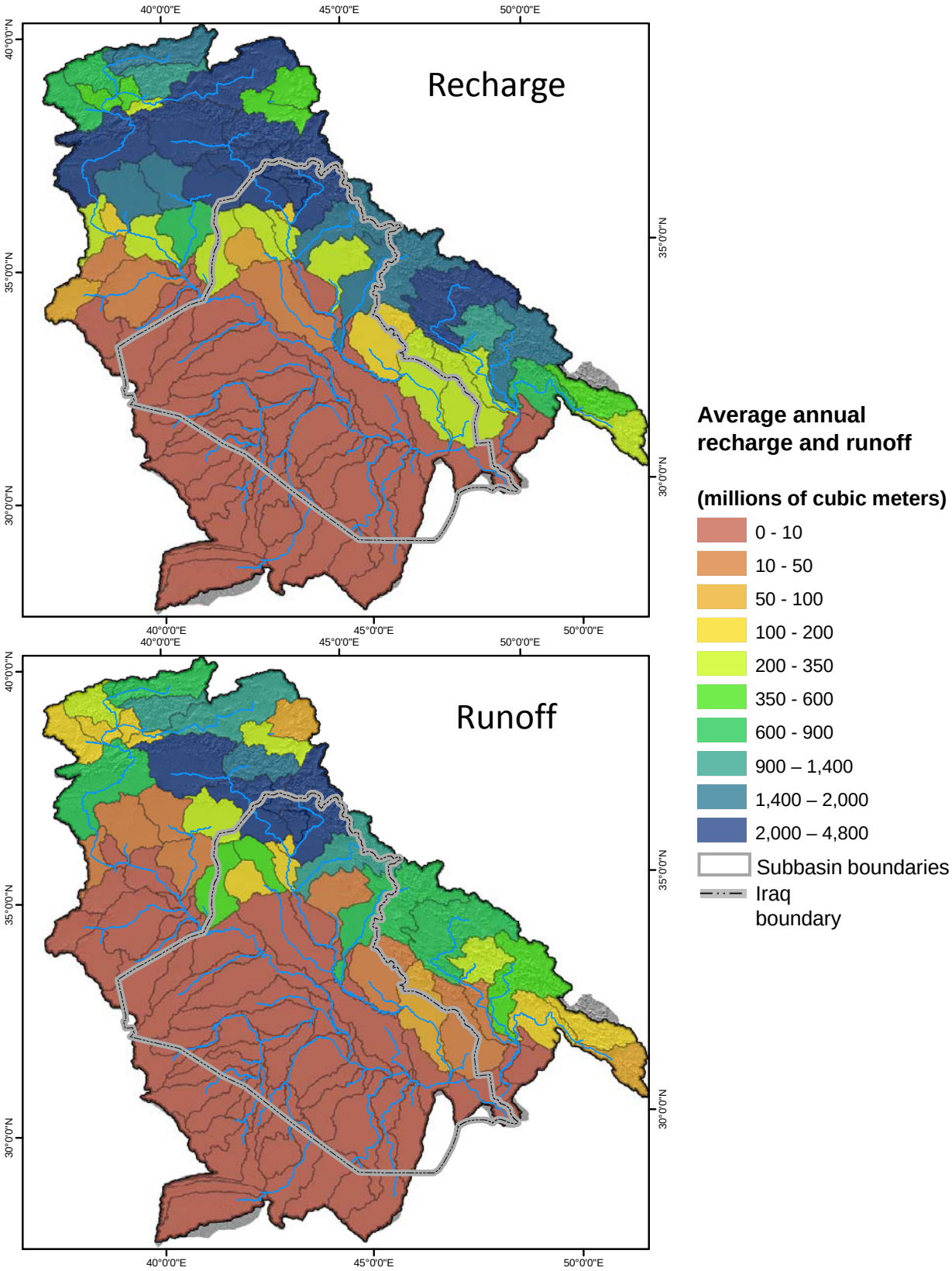

Figure 15. Maps of average annual recharge and runoff as volumes for each subbasin in the Tigris Euphrates River system.

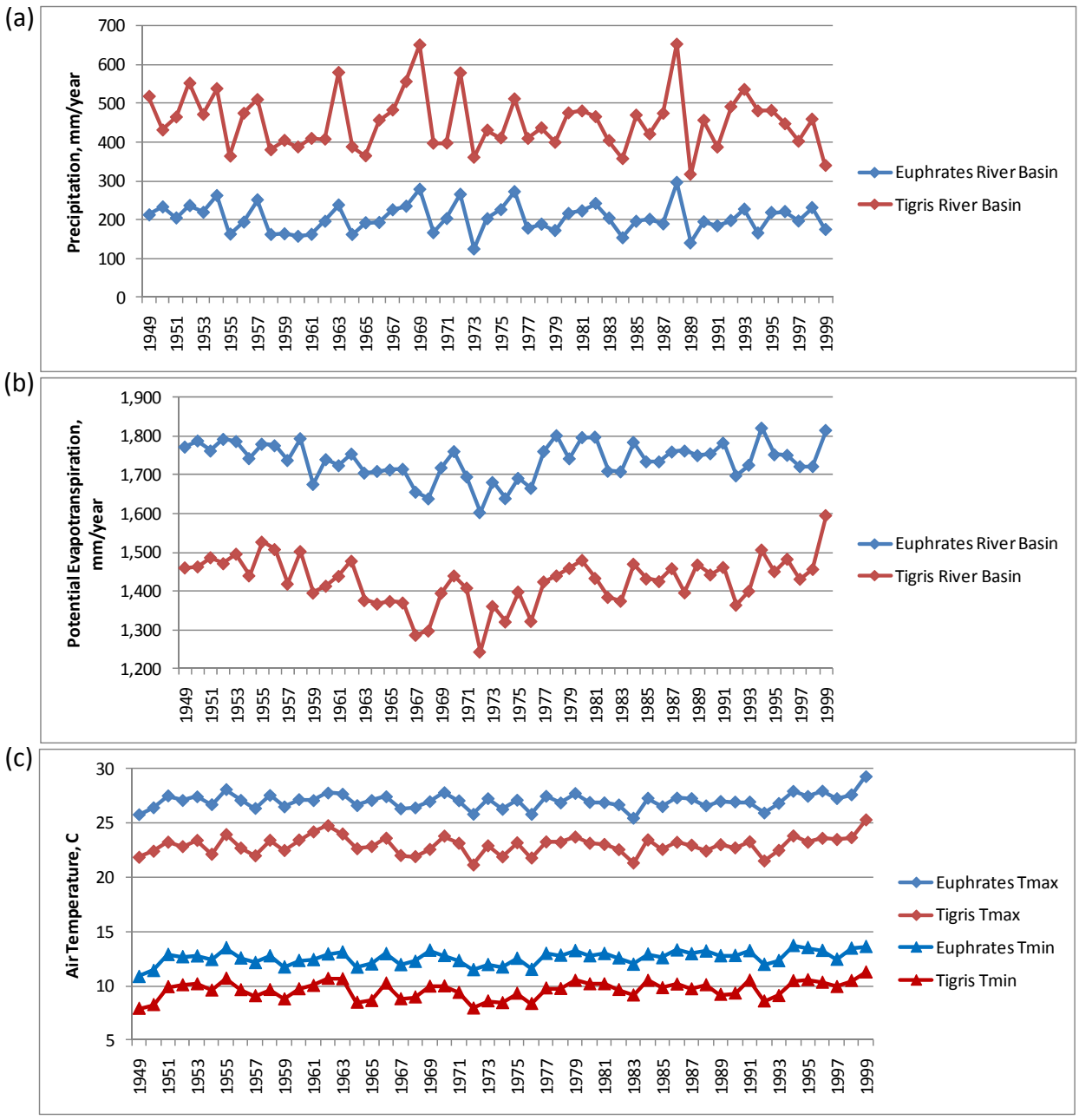

Figure 16. Annual results for 1949-1999 for the Euphrates River Basin and the Tigris River Basin for (a) precipitation, (b) potential evapotranspiration, and (c) maximum and minimum air temperature.

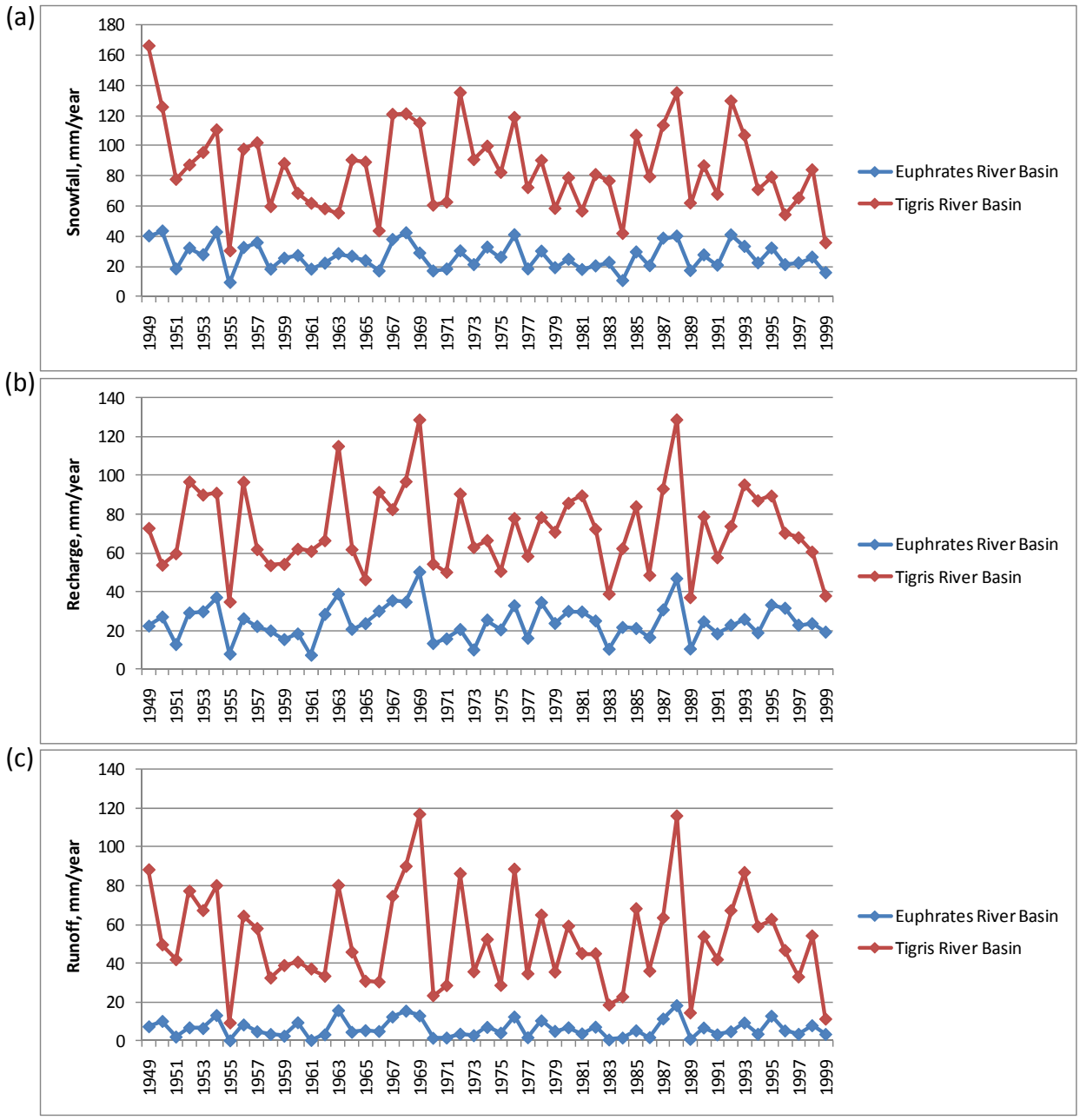

Figure 17. Annual results for 1949-1999 for the Euphrates River Basin and the Tigris River Basin for (a) snowfall, (b) recharge, and (c) runoff.

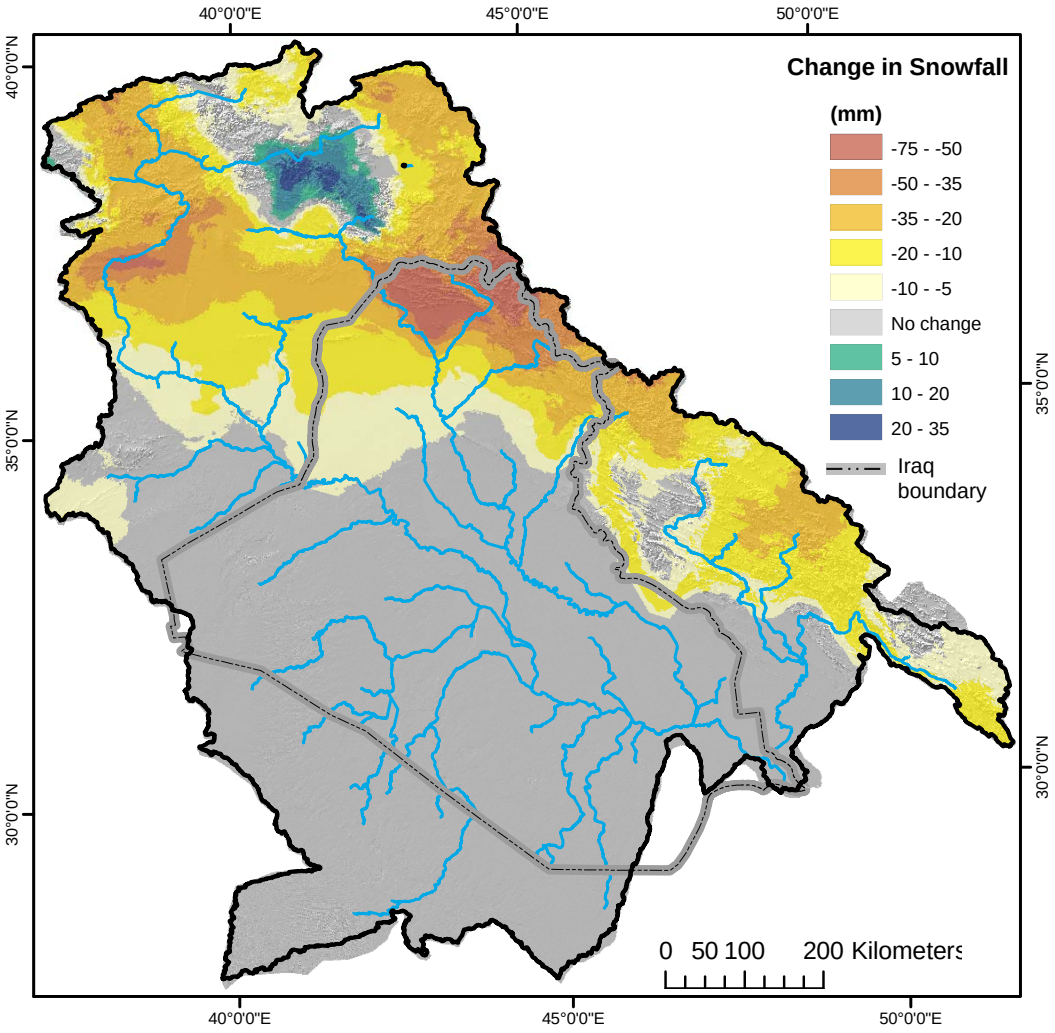

Figure 18. Map of the change in snowfall over the 50-year period from 1949-1999 for the Tigris Euphrates River System.

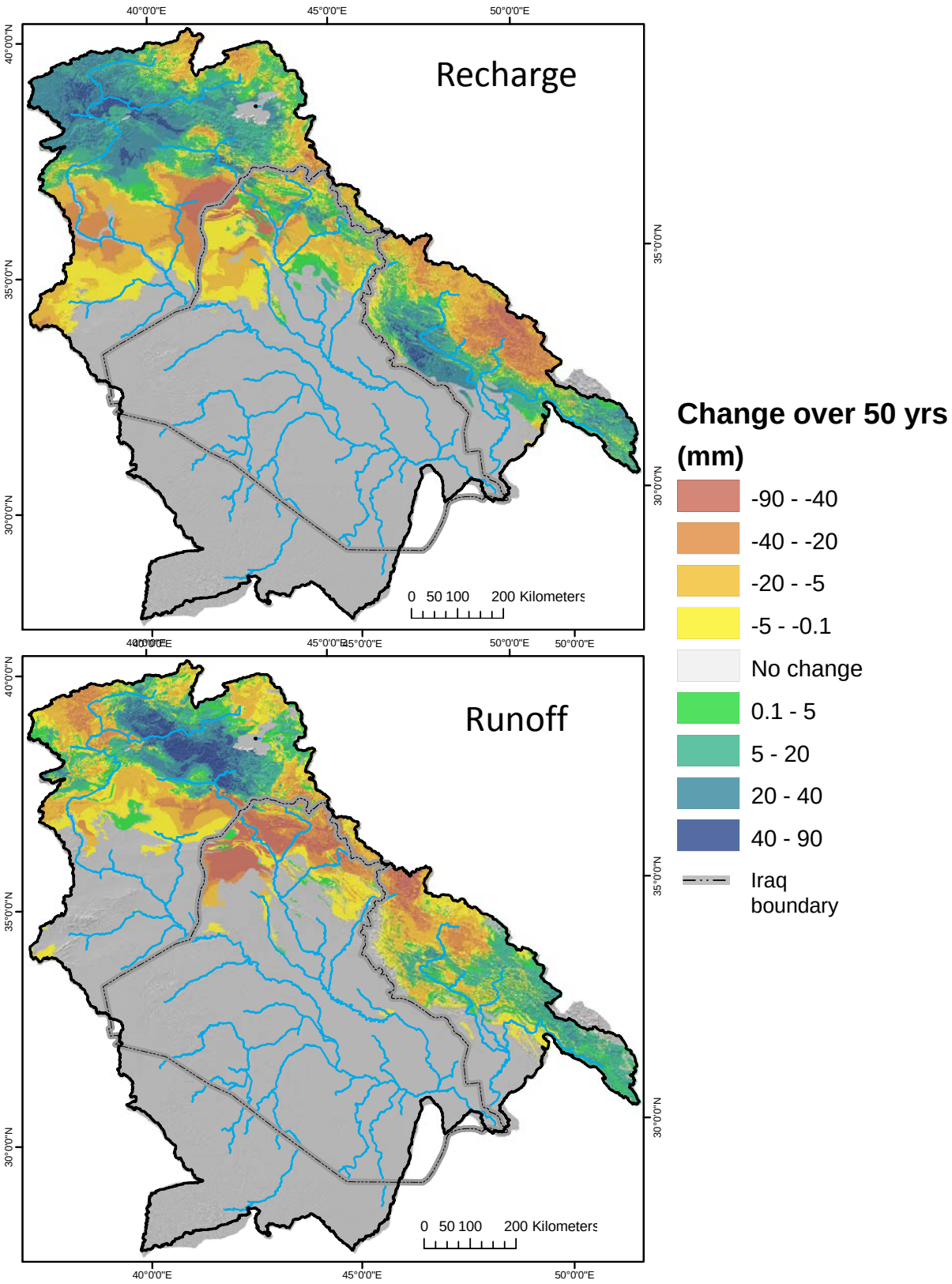

Figure 19. Map of the change in recharge and runoff over the 50-year period from 1949-1999 for the Tigris Euphrates River System.

Table 1. Unimpaired streamflow gages in the Tigris and Euphrates River System.

Gage name	Latitude (decimal degrees)	Longitude (decimal degrees)	Elevation (meters)	Catchment area (km2)	Period of record
Euphrates at Bagistas	39.450	38.483	1,277	15,562	1975-1982
Euphrates at Murat	38.692	39.929	1,000	25,447	1975-1985
Khazir at Manquba	36.300	43.550	549	2,900	1944-1994
Khabu at Zakho	37.133	42.683	254	3,500	1958-1988

Table 2. General description of lithologic units used in the Basin Characterization Model, including initial estimates of hydraulic conductivity and final calibrated saturated hydraulic conductivity.

[mm/day, millimeters per day]

General lithologic description	Calibrated saturated hydraulic conductivity (mm/day)	Initial estimate of hydraulic conductivity (mm/day)
Active marsh deposits	100.0	500
Aeolian	4,000.0	10,000
Argillaceous marl, argillaceous limestone, and shale	20.0	500
Bammu Conglomerate	50.0	10,000
Carbonate	30.0	10,000
Carbonate	30.0	5,000
Carbonate	30.0	1,000
Carbonate	30.0	8
Carbonate, shale	10.0	500
Chalky and crystalline limestones with marl and chert	1.0	10
Depression-fill deposits	0.1	500
Dolomite and dolomitic limestone with gypsum and anhydrite beds	5.0	1,000
Dolomite and finely recrystallised limestone	20.0	1
Dolomites, limestone, argillaceous chalky limestone, phosphorite	1.0	500
Dolomitized limestone with shale	10.0	500
Estuarine sabkha	2.0	100
Evaporites (gypsum, marl, and limestone)	5.0	5,000
Evaporites (gypsum, marl, and limestone)	20.0	1,000
Evaporites (gypsum, marl, and limestone) with (impermeable) mudstone	0.5	500
Evaporites (gypsum, marl, and limestone) with (impermeable) mudstone	1.0	50
Fine-coarse grained sand and sandstone	100.0	1,000
Flood plain and crevasse splays	1,000.0	500
Flood plain and fluvial deposits	2,500.0	20,000
Gravels and sands with varying amounts of clay	1,500.0	10,000
Gypcrete deposits	1.0	100
Horan gravels	1,500.0	10,000
Inland sabkha	5.0	2,400
Intrusive	50.0	50
Limestone and agillaceous limestone, well-bedded	0.5	1,000
Limestone and chalky limestone	5.0	1,000
Limestone with impermeable clay and marl	1.0	500
Limestone with impermeable clay and marl	1.0	5
Limestone, dolomite	5.0	10
Limestone, dolomite, interbedded with marl	10.0	5,000
Limestone, generally dolomitised and recrystallised	20.0	10,000
Limestone, shale	40.0	1,000
Limestone, shale	5.0	11
Limestone, shale	50.0	1
Lower clastic, upper carbonate	2.0	50
Marl, argillaceous limestone, siltstone, conglomerate	20.0	5,000
Marl, marly limestone, limestone, dolomite	10.0	10,000
Metamorphic	10.0	1,000
Metamorphic	1.0	8
Mudstone	3.0	1,000
Mudstones (impermeable)	0.2	0
Polygenetic deposits	20.0	500
Red bed series, shale, sandstone, conglomerate	20.0	500
Sand, gravel, and conglomerate	200.0	1,000
Sandstone and shale beds	10.0	833
Sandstone, shale	1.0	500
Shale	1.0	1
Shale, carbonate	5.0	50
Shale, sandstone	10.0	167
Sheet-run-off deposits	0.1	0
Slightly dolomitized limestone	5.0	10,000
Slightly dolomitized limestone	5.0	5,000
Slightly dolomitized limestone	5.0	10
Tidal flat deposits	0.1	500
Volcanic	20.0	1,000

Table 3. Average annual water balance components for the Tigris and Euphrates River basins and countries within the Tigris Euphrates River System.

	Precipitation		Potential Evapotranspiration		Snowfall		Recharge		Runoff	
Country or River Basin	millimeters	millions of cubic meters	millimeters	millions of cubic meters	millimeters	millions of cubic meters	millimeters	millions of cubic meters	millimeters	millions of cubic meters
Tigris River Basin	454	126,703	1,426	398,316	85	23,801	73	20,255	52	14,608
Euphrates River Basin	204	128,958	1,737	128,958	26	16,692	24	15,261	6	4,039
Turkey	600	115,418	1,062	204,181	185	35,435	136	26,110	55	10,601
Syria	207	24,065	1,465	170,146	14	1,602	44	5,127	1	133
Iraq	206	86,909	1,842	777,241	17	7,291	17	6,977	15	6,445
Iran	376	60,158	1,810	289,437	103	16,506	65	10,419	19	3,036
Saudia Arabia	116	16,573	1,914	273,809	0	21	0	-	-	-